A STUDY OF CATALYTIC NANOCARBON SYNTHESIS BY MEANS OF QUANTUM MECHANICAL METHODS

A THESIS SUBMITTED TO
THE GRADUATE SCHOOL OF NATURAL AND APPLIED SCIENCES
OF
MIDDLE EAST TECHNICAL UNIVERSITY

BY

İLKER TEZSEVİN

IN PARTIAL FULFILMENT OF THE REQUIREMENTS
FOR
THE DEGREE OF MASTER OF SCIENCE
IN
CHEMICAL ENGINEERING

JANUARY 2012

Approval of the thesis:

A STUDY OF CATALYTIC NANOCARBON SYNTHESIS BY MEANS OF QUANTUM MECHANICAL METHODS

submitted by **İLKER TEZSEVİN** in partial fulfillment of the requirements for the degree of **Master of Science in Chemical Engineering Department, Middle East Technical University** by,

Prof. Dr. Canan Özgen
Dean, Graduate School of **Natural and Applied Sciences** _____

Prof. Dr. Deniz Üner
Head of Department, **Chemical Engineering** _____

Prof. Dr. Işık Önal
Supervisor, **Chemical Engineering Dept., METU** _____

Examining Committee Members:

Prof. Dr. Hayrettin Yücel
Chemical Engineering Dept., METU _____

Prof. Dr. Işık Önal
Chemical Engineering Dept., METU _____

Prof. Dr. Göknur Bayram
Chemical Engineering Dept., METU _____

Prof. Dr. Şinasi Ellialtıoğlu
Physics Dept., METU _____

Dr. Derya Düzenli
Maden Analizleri ve Teknolojisi, MTA _____

Date: 17.01.2012

I hereby declare that all information in this document has been obtained and presented in accordance with academic rules and ethical conduct. I also declare that, as required by these rules and conduct, I have fully cited and referenced all material and results that are not original to this work.

Name, Last name: İLKER TEZSEVİN

Signature:

ABSTRACT

A STUDY OF CATALYTIC NANOCARBON SYNTHESIS BY MEANS OF QUANTUM MECHANICAL METHODS

Tezsevin, İlker

M.Sc., Department of Chemical Engineering

Supervisor: Prof. Dr. Işık Önal

January 2012, 71 pages

Throughout this thesis work, surface nanocarbon synthesis on metal catalyst surfaces was investigated as the first step of carbon nanotube production mechanism. Study was aimed to make a comparison between the performances of selected catalyst surfaces and to find most probable mechanism for the nanocarbon synthesis on the metal catalyst surface. Formation of nanocarbon from the acetylene as carbon source on the selected Fe(111), Ni(111) and Ni(100) surfaces were studied by means of quantum mechanics. Density functional theory (DFT) was implemented periodically by using Vienna Ab-initio Simulation Package (VASP) code for the computations required. Relative energy profiles of the interested mechanisms were generated by the usage of equilibrium geometry calculations, climbing image nudged elastic band (CI-NEB) calculations and transition state calculations. Formation step of surface nanocarbon, with the decomposition of the carbon source, is the rate determining step of carbon nanotube production. Therefore, results of the nanocarbon synthesis study were

related to carbon nanotube synthesis. For the mechanistic study, surface-acetylene complex was obtained by the adsorption of the acetylene on the chosen catalyst surface. Then three different mechanisms were studied for the dehydrogenation process. These processes were named as direct hydrogen-hydrogen interaction, hydrogen atom desorption and surface-hydrogen interaction methods. Among these methods surface-hydrogen interaction methods resulted in minimum activation barriers for all three surfaces used and said to be the most probable mechanism. Finally, relative energy profiles of the mechanisms were compared for the Fe(111), Ni(100) and Ni(111) surfaces and performance of Fe(111) for CNT synthesis was found better than the others.

Keywords: DFT, Carbon Nanotubes, Mechanism, Catalysis, VASP

ÖZ

KUANTUM MEKANİK METOTLAR KULLANILARAK KATALİTİK NANOKARBON SENTEZİ ÇALIŞMASI

Tezsevin, İlker

Yüksek Lisans, Kimya Mühendisliği Bölümü

Tez Yöneticisi: Prof. Dr. Işık Önal

Ocak 2012, 71 sayfa

Bu tez çalışmasında metal katalizör yüzeyi üzerinde nanokarbon sentezi karbon nanotüp sentezinin ilk aşaması olarak incelenmiştir. Çalışma, seçilen metal katalizör yüzeylerinin performanslarının kıyaslanmasını ve yüzey karbon sentezi için en muhtemel mekanizmanın bulunmasını amaçlamıştır. Seçilen Fe(111), Ni(100) ve Ni(111) yüzeyleri üzerinde karbon kaynağı olarak asetilen kullanılarak nanokarbon oluşumu için kuantum mekanik yöntemlerle çalışılmıştır. Gereken hesaplamalar için yoğunluk fonksiyonel teorisi (DFT) periyodik olarak Vienna Ab-initio Simulation Package (VASP) yazılımı kullanılarak uygulanmıştır. İlgilenilen mekanizmaların göreli enerji grafikleri denge geometrisi, CI-NEB ve geçiş hali hesaplarının sonuçları kullanılarak oluşturulmuştur. Karbon kaynağının ayrıştırılmasıyla yüzey karbonu oluşum aşaması karbon nanotüp sentezi için hız belirleyici adımdır. Bu yüzden nanokarbon sentezi çalışmasında elde edilen sonuçlar karbon nanotüp senteziyle ilişkilendirilmiştir. Mekanizma çalışmaları için asetilenin seçilen metal yüzeylere adsorpsiyonuyla yüzey-

asetilen kompleksi elde edilmiştir. Sonrasında, dehidrojenasyon aşaması için üç farklı mekanizma çalışılmıştır. Çalışılan bu mekanizmalar direkt hidrojen-hidrojen etkileşimi, hidrojen atomu koparma ve yüzey-hidrojen etkileşimi mekanizmaları olarak isimlendirilmiştir. Bu mekanizmalar arasından yüzey-hidrojen etkileşimi mekanizması tüm yüzeyler için en düşük aktivasyon bariyerlerini vermiştir ve en muhtemel mekanizma olduğu söylenmiştir. Son olarak, mekanizmaların göreli enerji grafikleri Fe(111), Ni(100) ve Ni(111) yüzeyleri için kıyaslanmış ve Fe(111) yüzeyinin performansının karbon nanotüp sentezi için diğerlerinden daha iyi olduğu bulunmuştur.

Anahtar Kelimeler: DFT, Karbon Nanotüp, Mekanizma, Kataliz, VASP

To My Family

ACKNOWLEDGEMENTS

First of all, I would like to thank my supervisor Prof. Işık Önal for his invaluable guidance, encouragement and helpful suggestions during my research in METU.

I would also like to thank to Dr. M. Ferdi Fellah and Dr. M. Oluş Özbek for sharing their knowledge on computational catalysis. Also I would like to thank Deniz Onay and Emine Kurnaz for their helps and friendship during my studies.

I thank and acknowledge my friends Gökhan Çelik, Duygu Gerçeker, Şule Kalyoncu and Miray Gülbiter for their friendship and all of the times we spent together. I especially thank Yasemin Coşkun for her supportive attitude, patience and for many things that I cannot put into words.

I would like to express my special thanks to my parents Mehmet Tezsevin and Fatma Nur Tezsevin for their constant support, patience and sincere love without any expectation.

The Scientific and Technological Research Council of Turkey (TÜBİTAK) is also acknowledged for the partial financial support under graduate scholarship of TÜBİTAK BİDEB (2228).

TABLE OF CONTENTS

LIST OF FIGURES

FIGURES

CHAPTER 1

INTRODUCTION

In this thesis study catalytic synthesis of surface nanocarbons was studied by means of quantum mechanical methods. This study can be seen as the initial step of carbon nanotube production mechanism. Before giving the results of the study, some general information were given about catalysis phenomena, computational chemistry and carbon nanotubes as an introduction. Finally, objectives of the study were stated.

1.1. Catalysis

The catalysis phenomena can be defined by the behavior of substances named as catalysts that are increasing the rate of the reactions. Catalysts conserve their structures at the end of the reactions that they catalyzed (Inglezakis & Poulopoulos, 2006). To be able to see a catalytic process, one does not have to look for highly complex or secret projects. It is just enough to look human body. Human body can be seen as a biological factory that is using different enzymes as catalysts for the biological processes. Catalysts are being used in many different industrial areas like refining processes, synthesis of pharmaceuticals, polymers, fertilizers, paints, adhesives and fine chemicals and also in waste treatment processes. Some numbers can be given to emphasize the importance of catalysis. Process involving catalyst usage holds 20% of the Gross Domestic Product of the United States. This value corresponds to 80-90% of

the all chemical processes and value of the products of these processes is more than $1800 billion (Howard, Morris, & Sunley, 2007) (Neurock, 1997).

Catalysts only change the rate of the reaction by reducing the activation barrier for the rate determining step(s). It is not possible to conduct a thermodynamically impossible reaction by using catalyst; however catalysts have no effect on the thermodynamics of the reaction. Catalysts only enhance the rate if the reaction is already happening (maybe with an extremely small rate that cannot be recognized). Also, catalyst has no effect on the equilibrium composition. Catalyst treats forward and backward reaction rates with the same extent. Furthermore, composition and structure of the catalyst remain same at the end of the catalytic cycle. The reason that catalysts increase the amount of desired product is the change in the overall selectivity. Hence, if the activation barrier in the desired pathway decreases, reaction rate for the path will be increased and process will shift to that side. As a result, amount of desired product will be increased. (Inglezakis & Poulopoulos, 2006; Smith & Notheisz, 1999).

It is possible to categorize types of catalysts as (also seen in Figure 1):

- Biological Catalysts
- Homogeneous Catalysts
- Heterogeneous Catalysts

1.1.1. Biological Catalysts

Biological catalysts are simply enzymes that are showing catalytic activity inside or outside of the living biological organisms. Enzymes are generally composed of proteins and they are needed to be able to handle nearly all reactions in living cells. Biological catalysts are also preferred for fine chemical, pharmaceutical and food production processes (Howard, et. al., 2007).

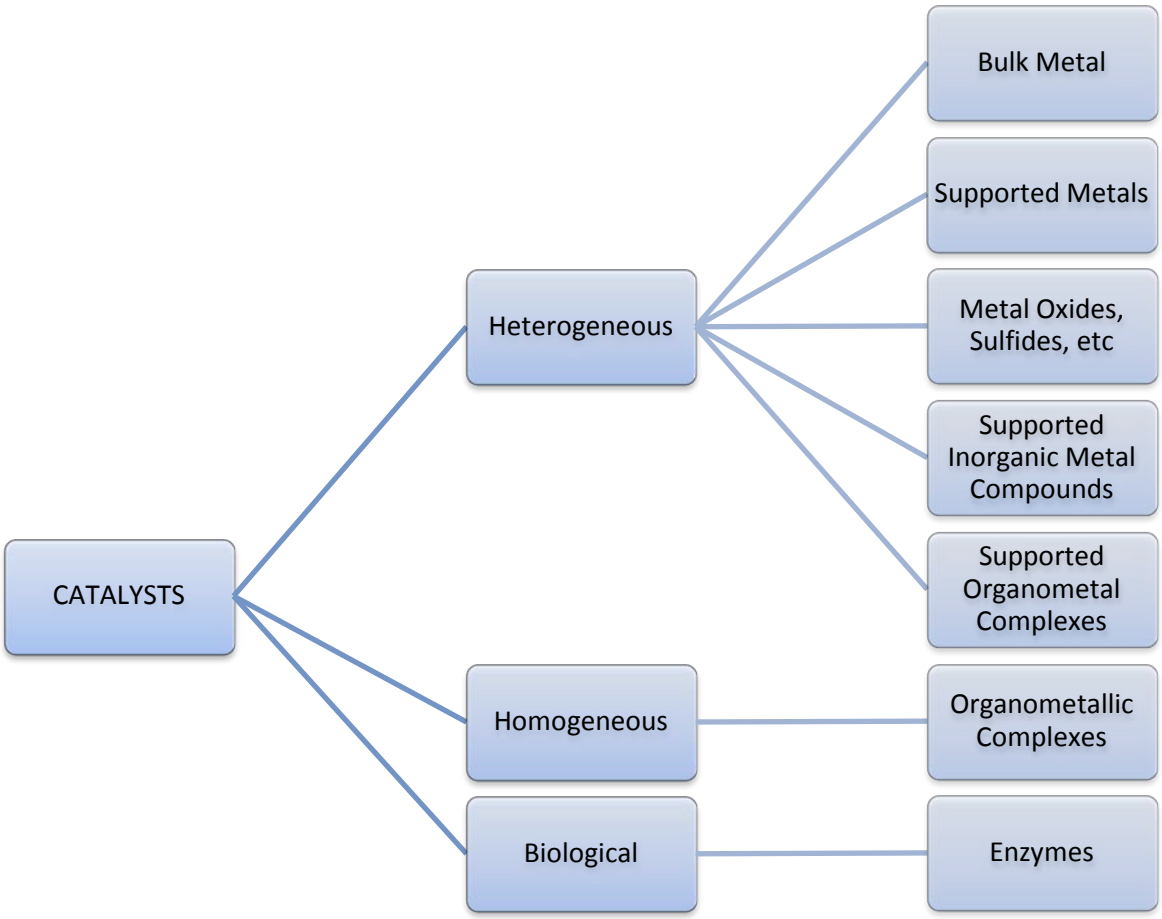

Figure 1: Types of catalysts

1.1.2. Homogeneous Catalysts

Homogeneous catalysts are the catalysts that are in the same phase with the reactants of the reaction. These kinds of catalysts are generally used for the liquid phase reactions. Homogeneous catalysts are easy to study however removal of the catalyst from the products at the end of the reaction to be able to reuse in the following batches may generate some problems for the industrial applications. Generally, homogeneous catalysts are preferred for commodity and fine chemical production processes (Howard, et. al., 2007; Smith & Notheisz, 1999).

1.1.3. Heterogeneous Catalysts

Heterogeneous catalysts are catalysts that are in a different phase than the phase of the reactants of the reaction. Generally heterogeneous catalysts are in solid state and used for liquid or gas phase reactions. When it is investigated, it can be seen that 90% of refining process uses heterogeneous catalyst. This value is 75% for all catalytic processes (Howard, et. al., 2007; Inglezakis & Poulopoulos, 2006).

As it is stated before, catalysts leave the reaction with their initial form. Process involving insertion of catalyst to the reaction and leaves the system is called as catalytic cycle. Catalytic cycle basically involves following steps:

- Activation of the reactive sites of the catalyst,
- Adsorption and diffusion of reactants to the active sites of the catalyst,
- Activation of the reactants,
- Bond break down and formation of new bonds to generate new products,
- Completion and desorption of the products from the catalyst.

1.2. Computational Chemistry

Computational chemistry can be defined as the combination of mathematical methods and fundamental physical laws in scope of chemical problems with the usage of computers as experimental tool. Aim of computational chemistry is somewhat different than the goals of classical theoretical chemistry. Unlike classical theoretical chemistry, computational chemistry is interested in the solution of the problem and obtaining the results instead of formulating new methods (Jensen, 2007). Computational chemistry has started to be an important part of the experimental chemistry also. In many experimental studies, including theses and books, computational chemistry is using to be able to support experimental results and to get information about the molecular

structure. Associated with the development of powerful computer technology, computational chemistry is now being applied by majority of modern chemists in their works (Heine, et. al., 2009).

In the present day, by the aid of computational chemistry it is possible

- to have an idea about the molecular structure of the interested materials,
- to examine energies of molecules and transition states
- to understand stability and chemical structures,
- to examine surface intermediates in the reactions, especially important for the cases including rapid formation and disappearance that cannot be followed by experimental methods,
- to reveal reaction pathways,
- to predict some properties of materials before synthesis process with in cheaper and quicker manner (Heine, et. al., 2009; Lewars, 2003; Young, 2001)

Computational quantum chemical methods can be classified as follows:

- Ab-initio Methods
    - Ab-initio Hartree-Fock Methods
    - Ab-initio Correlated Methods
        - Configuration Interaction Methods
        - Multi-Configuration Methods
        - Coupled Clusters Methods
        - Pair Methods
        - Perturbational Methods
- Semiempirical Methods
- Density Functional Methods

- Molecular Mechanics
- Molecular Dynamics and Monte Carlo Simulations
  (Rode, et. al., 2007; Lewars, 2003)

In this work only density functional theory (DFT) is examined in detail.

1.2.1. Density Functional Theory (DFT)

Density functional theory is the one of the best quantum mechanical methods in computational chemistry. Especially for transition metals, implementation of density functional theory increases accuracy of the results without increasing the computational time required. DFT differs from other methods with the usage of electron density, instead of wave function, in the solution of Schrödinger equation (in other words getting information about the chemical systems) (Nagy, 1998; Rode, et. al., 2007). Development of density functional theory comes from the assumption made by Thomas and Fermi and the proofs of Hohenberg and Kohn, and Kohn and Sham (Parr & Yang, 1994; Varga & Driscol, 2011). According to assumption of Thomas "*Electrons are distributed uniformly in the six-dimensional phase space for the motion of an electron at the rate of two for each* h^3 *of volume*" and effective potential field can be found by using nuclear charge and electron distribution (Parr & Yang, 1994). The first theorem for the foundations of density functional theory obtained by the work of Hohenberg and Kohn and states that "*The ground-state energy from Schrödinger's equation is a unique functional of the electron density".* Second theorem, by Hohenberg and Kohn, states that "*The electron density that minimizes the energy of the overall functional is the true electron density corresponding to the full solution of the Schrödinger equation"* (Sholl & Steckel, 2009). Kohn and Sham stated that the many-electron problem can be altered with an equivalent set of self-consistent single particle equations (Varga & Driscol, 2011).

Wave function used for the solution of Schrödinger equation by other quantum mechanical methods is just a mathematical construct. However electron density used in the density functional method is a physical characteristic of all molecules.

It can be stated that how electron density can be used to define a system as:

- The number of electron can be obtained from the integral of the density
- The position of the nuclei can be obtained from the cups in the density
- The corresponding nuclear charges can be obtained from the height of the cups (Jensen, 2007)

1.2.2. Formulation of Density Functional Theory

As it is stated before density functional theory is used to solve Schrödinger equation by functional of electron density. To be able to formulate this process it is better to start with Schrödinger equation:

$$\hat{H}\Psi = E\Psi \quad (1)$$

In Schrödinger equation $\hat{H}$ represents Hamiltonian operator and Ψ represents wave function.

Hamiltonian operator consists of external potential due to M nuclei operator ($\hat{\upsilon}_{ext}$), kinetic energy operator ($\hat{T}$) and electron-electron repulsion operator ($\hat{V}_{ee}$) and can be extended as:

$$\hat{H} = \hat{\upsilon}_{ext} + \hat{T} + \hat{V}_{ee} \quad (2)$$

where

$$\hat{v}_{ext} = -\sum_{i=1}^{N}\sum_{A=1}^{M}\frac{Z_A}{|\vec{R}_A-\vec{r}_i|} \quad (3)$$

$$\hat{T} = -\frac{1}{2}\sum_{i=1}^{N}\nabla_i^2 \quad (4)$$

$$\hat{V}_{ee} = \sum\sum_{i<j}\frac{1}{r_{ij}} \quad (5)$$

Wave function in Schrödinger equation is the function of position vectors ($\vec{r}_N$) and spin coordinates (s_N) of all N electrons. However spin coordinates will be taken implicit and not shown in the equations. According to this explanation, wave function can be shown as:

$$\Psi = \Psi(\vec{r}_1, \vec{r}_2, \vec{r}_3, \dots, \vec{r}_N) \quad (6)$$

Although Hamiltonian operator includes another term, nuclear-nuclear repulsion (V_{NN}), this part will be added at the stage of getting the total energy.

To be able to solve Schrödinger equation density functional theory does not uses N-electron wave functions like other methods. In density functional theory electron density is used to be able to deal with Schrödinger equation. Electron density can be written as:

$$\rho(\vec{r}) = N\langle\Psi|\delta(\vec{r}-\vec{r}_i)|\Psi\rangle \quad (7)$$

This equation can be written for a singular expectation value as:

$$\rho(\vec{r}_1) = N\int d\vec{r}_2 d\vec{r}_3 \dots d\vec{r}_N |\Psi(\vec{r}_1, \vec{r}_2, \vec{r}_3, \dots, \vec{r}_N)|^2 \quad (8)$$

By using this information, total energy can be written as:

$$E = \langle\Psi\big|\hat{H}\big|\Psi\rangle = \int v_{ext}(\vec{r})\rho(\vec{r})d\vec{r} + \langle\Psi\big|\hat{T}+\hat{V}_{ee}\big|\Psi\rangle \quad (9)$$

According to equation (9) energy is a functional of external energy and electron density. Also for a given external potential of ν, ground state energy can be written as:

$$E = E_{\upsilon}[\rho] \tag{10}$$

If equation (10) is extended:

$$E = E_{\upsilon}[\rho] = \int \upsilon(\vec{r})\,\rho(\vec{r})d\vec{r} + \langle\Psi\left|\hat{T} + \hat{V}_{ee}\right|\Psi\rangle = \int \upsilon(\vec{r})\,\rho(\vec{r})d\vec{r} + F[\rho] \tag{11}$$

where $F[\rho]$ is the universal functional, which is independent from external energy and same for all systems.

According to derivations of Kohn and Sham trivial energy found for any ρ^t is the upper limit for the exact ground state energy.

$$E \leq E_{\upsilon}[\rho^t] \tag{12}$$

Hohenberg-Kohn theorem explains the solution up to this point. Theorem defines a universal functional $F[\rho]$, but does not give an explanation or solution for this. Kohn-Sham procedure can be used to find universal functional and solve Schrödinger equation after this point (Seminario, 1995).

Kohn-Sham procedure starts with the assumption of the following Hamiltonian operator:

$$\hat{H}_{\lambda} = \hat{T} + \upsilon_{\lambda} + \lambda V_{ee} \tag{13}$$

Value of the λ in the equation of Hamiltonian changes between 0 and 1 (If λ is 0, then it means that the system is ideal with non-interacting electrons. If λ is 1, then that means that the system is real with the effect of ν_{ext}.). Also, $\rho(r)$ can be obtained from υ_{λ} according to Hohenberg-Kohn theorem. Then Schrödinger equation becomes:

$$\hat{H}_{\lambda}\Psi_{\lambda} = E_{\lambda}\Psi_{\lambda} \tag{14}$$

After obtaining this equation, Energy becomes:

$$E_\lambda = \langle \Psi_\lambda | \widehat{H}_\lambda | \Psi_\lambda \rangle = \int v_\lambda(\vec{r}) \rho(\vec{r}) d\vec{r} + \langle \Psi_\lambda | \hat{T} + \lambda V_{ee} | \Psi_\lambda \rangle \quad (15)$$

After further processing one can obtain the following formula:

$$E[\rho] = \int v_{ext}(\vec{r})\, \rho(\vec{r}) d\vec{r} + T_s + \int_0^1 \langle \Psi_\lambda | V_{ee} | \Psi_\lambda \rangle\, d\lambda \quad (16)$$

where T_s is kinetic energy of the non-interacting electron system, which is imaginary. However energy equation cannot be solved for λ again. To be able to simplify the equation further, define an exchange correlation energy term as the difference between the second integral in (16) and classical electron-electron interaction energy.

$$V_{classical}[\rho] = \frac{1}{2} \int \int d\vec{r}_1 d\vec{r}_2 \frac{\rho(\vec{r}_1)\rho(\vec{r}_2)}{|\vec{r}_1 - \vec{r}_2|} \quad (17)$$

$$E_{xc}[\rho] = \int_0^1 \langle \Psi_\lambda | V_{ee} | \Psi_\lambda \rangle\, d\lambda - \frac{1}{2} \int \int d\vec{r}_1 d\vec{r}_2 \frac{\rho(\vec{r}_1)\rho(\vec{r}_2)}{|\vec{r}_1 - \vec{r}_2|} \quad (18)$$

If (18) and (16) rearranged:

$$\int_0^1 \langle \Psi_\lambda | V_{ee} | \Psi_\lambda \rangle\, d\lambda = V_{classical} + E_{xc}[\rho] \quad (19)$$

$$E[\rho] = \int v_{ext}(\vec{r})\, \rho(\vec{r}) d\vec{r} + T_s + V_{classical}[\rho] + E_{xc}[\rho] \quad (20)$$

The final expression gives the total energy of the electronic system. In this equation all terms are known except exchange-correlation energy part.

If the relation of exchange correlation part is also known, then only thing left is the minimization of the total energy with respect to electron density. This final procedure gives Kohn-Sham equations:

$$\left[-\frac{1}{2}\nabla^2 + v_{ext} + v_{classical} + v_{xc} \right] \varphi_i = \varepsilon_i \varphi_i \quad (21)$$

where

$$v_{classical}(\vec{r}) = \int d\vec{r}' \frac{\rho(\vec{r}')}{|\vec{r}-\vec{r}'|} \quad (22)$$

$$v_{xc}(\vec{r}) = \frac{\delta E_{xc}[\rho(\vec{r})]}{\delta\rho(\vec{r})} \quad (23)$$

Exchange energy should be found by the usage of some approximations like local density approximation (LDA) or generalized gradient approximations. Detailed information about these 2 approximation models will be given later. Exchange energies according to these two methods were given as:

$$E_{xc}^{LDA} = \int \varepsilon_{xc}^{LDA}[\rho(\vec{r})]\rho(\vec{r})d\vec{r} \quad (24)$$

where $\varepsilon_{xc}^{LDA} = {E_{xc}}/{volume}$ which is the only function of the local electron density.

$$E_{xc}^{GGA}[\rho] = \int d\,\vec{r}\,\varepsilon_{ex}[\rho, |\nabla\rho|, \nabla^2\rho] \quad (25)$$

(Seminario, 1995)

1.2.3. Local Density Approximation (LDA)

Local density approximation is the approximation for the exchange correlation that is assuming the system is locally an electron gas like a homogeneous system. This assumption also involves the hypothesis that density is changing slowly. Since high accuracy calculations for exchange correlation may be achieved by the usage of homogeneous electron gas systems. LDA can also be used for inhomogeneous systems with this assumption. However, it does not mean that LDA can be valid for all systems. Especially for the description of molecules, LDA can face with some problems (Engel & Dreizler, 2011; Jensen, 2007; Rode, et. al., 2007).

1.2.4. Generalized Gradient Approximation (GGA)

Generalized gradient approximation considers the systems as non-uniform electron gas and relates exchange correlation of the system with both density and derivatives of the density. GGA method improves the results for the total energies of atoms, binding energies, vibrational frequencies and bond lengths (Filirri, et. al., 1996; Jensen, 2007).

1.3. Carbon Nanotubes

Carbon nanotubes were first discovered by Iijima in 1991 and became a very popular research subject for scientists. Carbon nanotubes are nano structural materials with high length to diameter ratio. C atoms in the structure of carbon nanotubes show sp^2 hybridization (Patel, et. al., 2011). They can be imagined like a graphene sheet that is rolled up to get an extended tubular structure. These tubular structures are divided into two types as single walled carbon nanotubes (SWCN) and multi walled carbon nanotubes (MWCN). Single walled carbon nanotubes are single tubes as it can be understood from their name. Multi walled carbon nanotubes contain concentric tubes with approximately 3.4Å spacing between their walls (Turner, 2008). Both single walled and multi walled carbon nanotubes have diameters of few nanometers and their length changes from nanometers to millimeters. Carbon nanotubes have unique electrical, optical, mechanical, structural and chemical properties however these properties may vary due to structure of the carbon nanotube (Rümmeli, et. al., 2010). Strength of carbon nanotubes is approximately 50 times greater than steel, their thermal conductivity is nearly twice of graphene and their density is nearly half of aluminum. According to reported data, carbon nanotubes are stable up to 3000K (Gasman, 2006). Common structures of single walled carbon nanotubes can be seen in Figure 2.

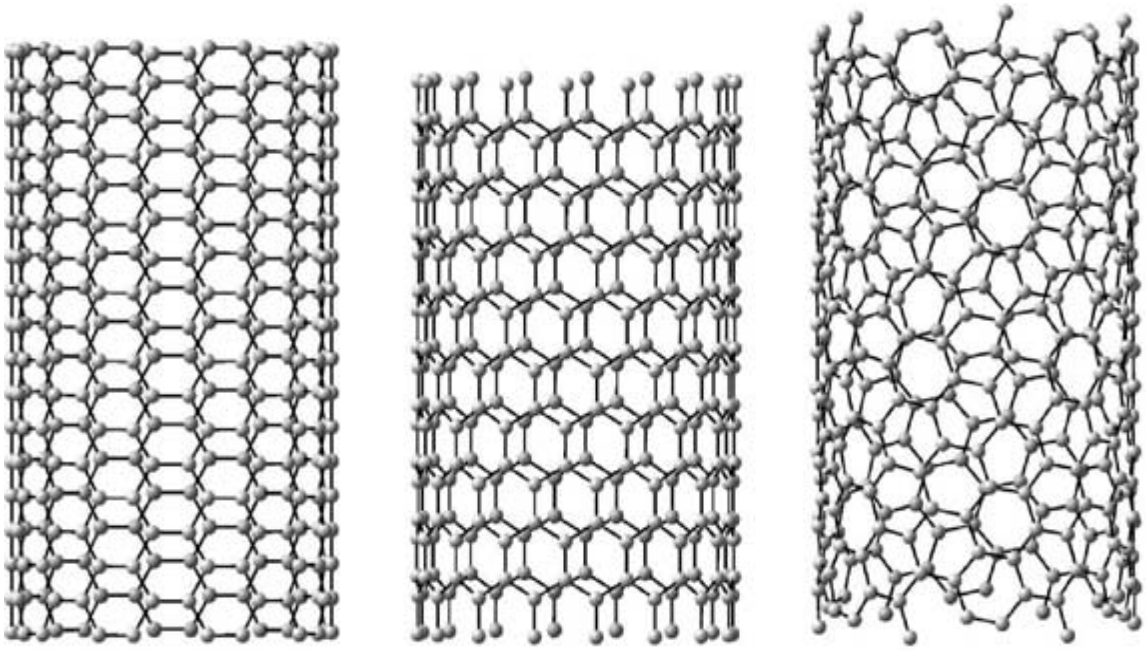

(A) (B) (C)

Figure 2: Different carbon nanotube structures: (A) armchair nanotube, (B) zigzag nanotube and (C) chiral nanotube (Popov, 2004)

Due to their magnificent properties, carbon nanotubes have lots of potential application areas. Actually, carbon nanotubes are readily being used in commercial products. Nowadays carbon nanotubes are being used for battery electrode additives, thermal management, packaging, composite materials and electron discharge applications requiring large amount of carbon nanotubes. Also carbon nanotubes are being used for scanning probe tips and medical appliances in smaller amounts. Future applications of carbon nanotubes can be examined under two headings as short-time (<10 years) and long-time (>10 years) applications according to expected time that they will be available on market. Short term applications of carbon nanotubes include battery and supercapacitor electrodes, processors, computer memories,

multifunctional composites, hydrogen storage, fuel cell electrodes and field emission displays and lighting with the usage of large amounts of carbon nanotubes. Applications requiring fewer amounts of carbon nanotubes for this section can be stated as single tip electron guns, multitip array X-ray sources, brush contacts, sensor devices, electromechanical memory device and thermal management systems. Long term applications requiring high amounts of carbon nanotubes can be stated in literature as power transmission cables, structural composites and photovoltaic devices. Nanoelectronics, flexible electronics, filtration and separation membranes, diagnostics devices and drug delivery systems are also long term applications of carbon nanotubes and they need fewer amounts of carbon nanotubes (Endo, et. al., 2008; Gasman, 2006; Joselevich E. J., et. al. , 2008; Patel, et. al., 2011).

Carbon nanotubes have many application areas and have been highly investigated during last two decades. However there are still important challenges for carbon nanotube production (Joselevich E. J., et. al., 2008). These challenges can be stated as:

- Effective and economical mass production techniques for the large scale synthesis of carbon nanotubes
- Selective production of carbon nanotube with desired structure and properties
- Management of substrate-carbon nanotube orientations
- Mechanism of carbon nanotube synthesis process

1.3.1. Production of Carbon Nanotubes

During last two decades, different synthesis methods have been proposed and studied for carbon nanotubes. Most popular and promising methods for the carbon nanotubes are arc discharge, laser ablation and catalytical chemical vapor deposition methods.

These methods are generally divided into two groups. Arc discharge and laser ablation methods are named as high temperature methods whereas chemical vapor deposition method is involved in medium temperature methods.

1.3.1.1. Arc Discharge Method

Arc discharge method can be used for the large scale production of carbon nanotubes. However method requires purification processes in spite of its simple usage. Method uses two graphite electrodes as one is located at cathode and the other one is located at anode side with 1mm spacing between. Anode graphite may also include metal catalyst within to be able to enhance reaction. Additionally, buffer gas, which is generally helium or argon, is used to cover the reaction medium. Method uses a flow of about 100 amperes and 20 volt to ignite an arc between anode and cathode electrodes to sublimate carbon from the electrodes. Then evaporated carbons condense to produce carbon nanotubes desired. During this process normally discharge temperature arises to 2000-3000°C. However, this temperature can be increased up to 6000°C (Loiseau, et al., 2006; Rümmeli, et. al., 2010). Scheme of carbon nanotube synthesis by arc discharge method can be seen in Figure 3.

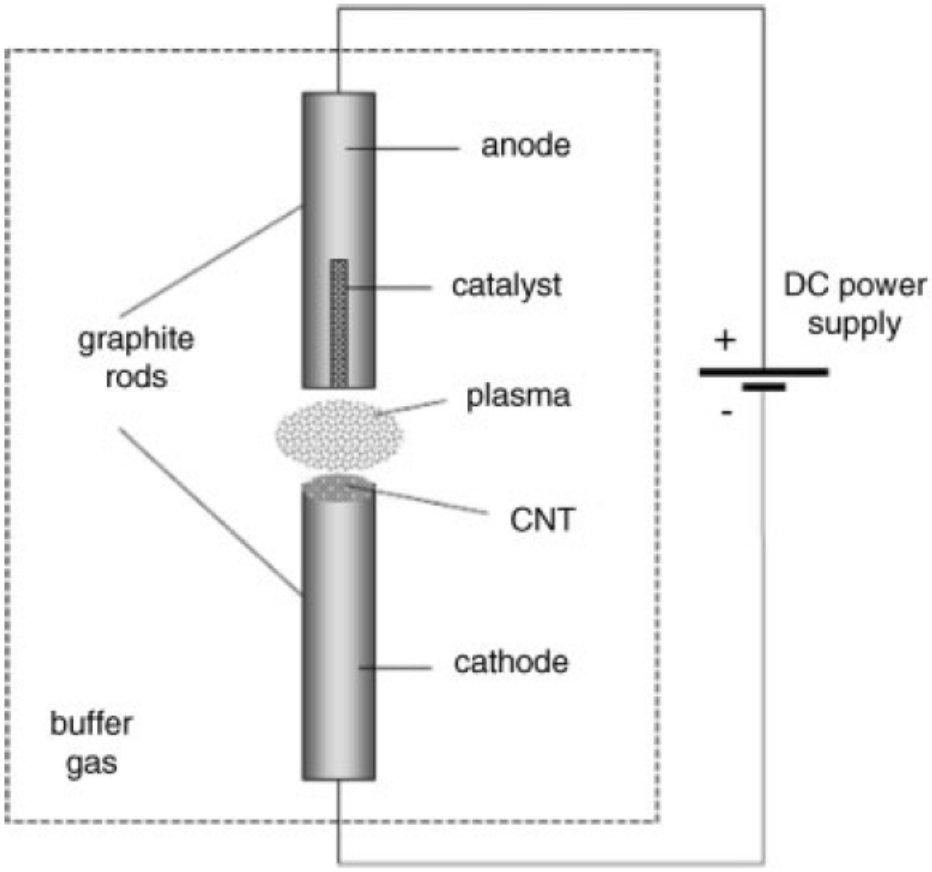

Figure 3: Arc-discharge method scheme for carbon nanotube synthesis (Rümmeli, et. al., 2010)

1.3.1.2. Laser Ablation Method

Laser ablation methods uses energy of pulsed laser to sublimate carbons of graphite target (including catalyst also) located into the furnace at 1200°C filled with helium or argon gas. Inert gas flow carries the carbons sublimated by laser pulse to the cold collector and carbon nanotubes accumulate on the surface of collector (Terrones & Terrones, 2007). Laser beam heats the target up to 3500K to be able to sublimate carbons of graphite. Laser ablation method has high yields and selectivity values,

additionally; quality and diameter of carbon nanotubes can be controlled in laser ablation method. Still, laser ablation method is not appropriate for the mass production of carbon nanotubes. Scheme of carbon nanotube synthesis by laser ablation method can be seen in Figure 4 (Rümmeli, et. al, 2010; Loiseau, et al., 2006).

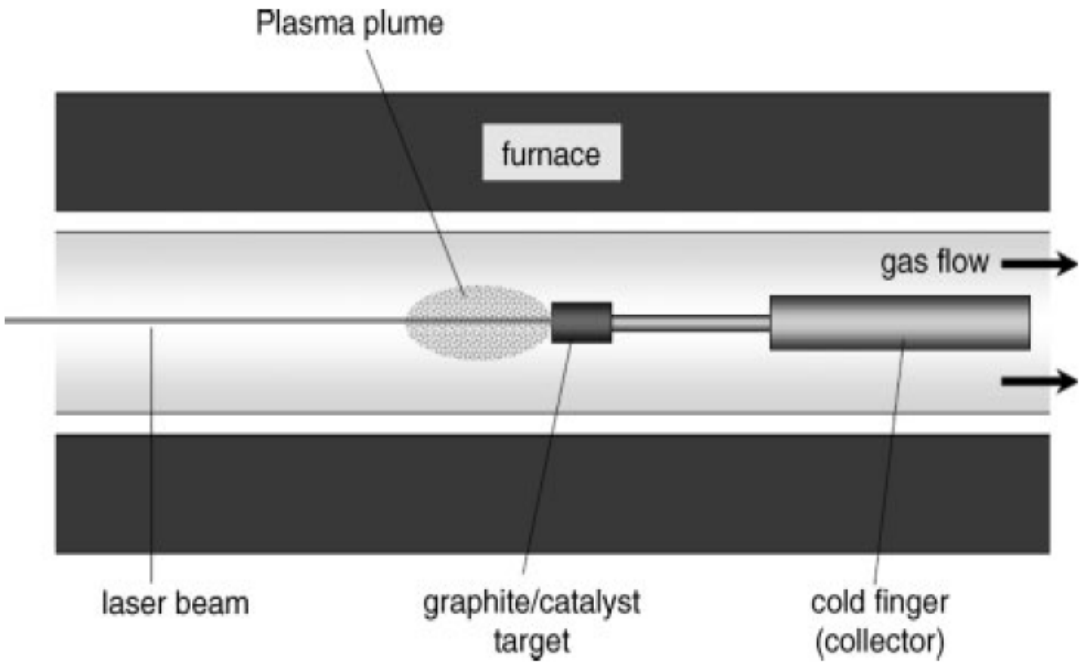

Figure 4: Laser ablation method scheme for carbon nanotube synthesis (Rümmeli, et. al., 2010)

1.3.1.3. Chemical Vapor Deposition

Chemical vapor deposition (CVD) method uses gaseous or volatile carbon sources and deposits them as carbon nanotubes on catalyst particles or pores. Chemical vapor deposition method operates between temperatures of 350-1000°C. During chemical vapor deposition method, volatile reactant interacts with the catalyst used and carbon nanotubes are formed from the carbons of the reactant deposits on the surface and gaseous products leaves the system. Setup for chemical vapor deposition method is

easier to construct than the previously discussed methods. Also method can be rescaled to be able to fulfill the industrial demands. Chemical vapor deposition method gives researcher ability to control the structure of carbon nanotube produced (Joselevich E. , et. al., 2008; Loiseau, et al., 2006; Rümmeli, et. al., 2010). Scheme of carbon nanotube synthesis by chemical vapor deposition method can be seen in Figure 5.

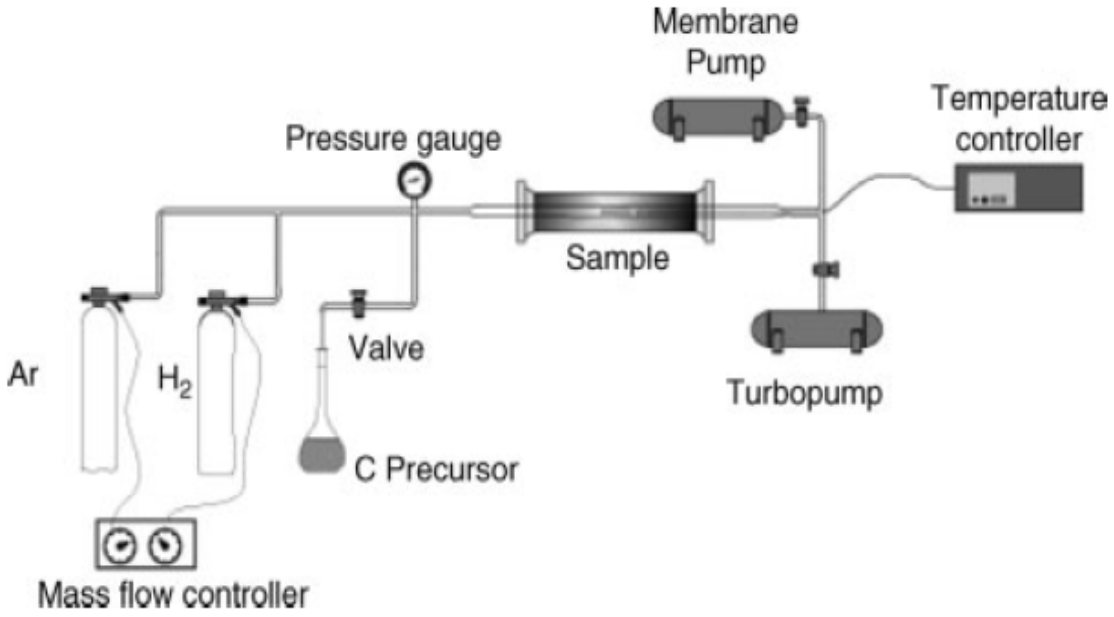

Figure 5: Chemical vapor deposition method scheme for carbon nanotube synthesis (Rümmeli, et. al., 2010)

1.4. Objectives of the Study

Due to their unique properties carbon nanotubes attracted the attention of researchers after their discovery. However lack of effective production methods for high capacity production and uncertainties in the mechanism of carbon nanotube production requires much more investigations. Objectives of this study can be stated in three sections:

- Primary objective of this thesis work is to study initial step of carbon nanotube production, surface nanocarbon formation, on various metal catalyst surfaces and to compare the performances of these metal catalyst surfaces carbon nanotube production. As it will be stated in the literature survey part, catalysts are required for carbon nanotube synthesis.
- Second objective of this study is to reveal the pathway (mechanism) through surface carbon formation. As well explained in the literature survey part of this thesis work, various pathways to synthesize carbon nanotubes are proposed according to experimental results, but these pathways are still not obvious. Carbon nanotube production mechanism, up to surface carbon synthesis, part will be examined in this work.
- The final objective of this study is to collaborate with the experimental work conducted in Sabancı University with the usage of same metal catalysts (Fe and Ni) and carbon source (acetylene) as a part of a TUBİTAK project.

CHAPTER 2

LITERATURE SURVEY

Carbon nanotubes have been investigated during last two decades, however mechanistic studies are still not sufficient to know what is exactly happening during carbon nanotube production. While there are excess amount of experimental studies for carbon nanotube production, there are very limited computational studies. Yet, there is no DFT study for the production mechanism of carbon nanotubes. Because of this reason, experimental literature was used for this thesis study.

Until their discovery by Iijima, carbon nanotubes were treated like waste products of carbon containing catalytic reactions which are inhibiting the desired reaction. After the work of Iijima, carbon nanotubes became a famous research subject all over the world (Lopez, et. al, 2001). Carbon nanotubes are synthetic materials. In another words, they cannot be found in nature (Journet & Bernier, 1998). However, there are various methods to synthesize carbon nanotubes. Mostly used synthesis methods can be stated as arc-discharge, laser ablation and (catalytical) chemical vapor deposition. Generally, arc discharge and chemical vapor deposition methods are being used for continuous processes today (Ying, et. al., 2011). Among them catalytical chemical vapor deposition method is the mostly used one due to low cost, high yields and easy scale up procedures. Results of arc discharge and laser ablation methods are also promising, however these two methods requires high amount of energy and high operating

temperatures around 3000°C (Ni, et al., 2006; Pirard, et. al., 2007). According to Dasgupta and coworkers, fluidized bed chemical vapor deposition method can be used for continuous synthesis of carbon nanotubes with promising rate and properties. In order to scale up this carbon nanotube synthesis process, mass transfer properties and kinetics of the reaction happening in the bed should be known clearly (Dasgupta, et.al., 2011; Ying, et. al., 2011).

Various catalysts can be used for the synthesis of carbon nanotubes. Most promising catalysts for carbon nanotube synthesis are known as Fe, Ni and Co nanoparticles; however, by using other transition metals like V, Cu, Mo, Mn and Cr small amounts of carbon nanotubes can also be produced. Addition of V and Mo are reported to increase the activity of Fe, Ni and Co catalysts. Usage of support materials like silica, alumina, magnesia and zeolites also changes the performances of the catalyst used (Popov, 2004; Vesselenyi, et al., 2001). According to study of Hernadi and coworkers, Fe catalyst gives better yield than Co catalyst for silica and Y supports (Hernadi, et. al., 2000). However when these two metals are used with alumina support, performance of Co is better than the performance of Fe catalyst (Tran, et. al., 2007). In the work of Jeong and coworkers, high carbon nanotube yield achieved by using Fe/Mo catalysts with magnesia support by using catalytical chemical vapor deposition method with the usage of acetylene/methane mixture as carbon feed source (Jeong, et. al., 2004). Also Tsoufis and coworkers claim that Fe/Ni (1:1) bimetallic catalyst with magnesia support as the promising catalyst for the mass production of carbon nanotubes (Tsoufis, et al., 2007). In the theoretical, molecular dynamic, study of Page and coworkers, Ni catalyst is found to show better performance than Fe when pure carbon is used (Page, et. al., 2010).

Other than the catalyst particles used, carbon sources are also very important for the carbon nanotube synthesis. Many carbon containing compounds like acetylene,

ethylene, propylene, acetone, *n*-pentane, methanol, toluene and methane can be used as carbon source for carbon nanotubes. In the work of Hernadi and coworkers, reactivity of various carbon sources were studied. According to their results (see Figure 6), acetylene was found to be best carbon source for carbon nanotube synthesis (Hernadi, et. al., 2000).

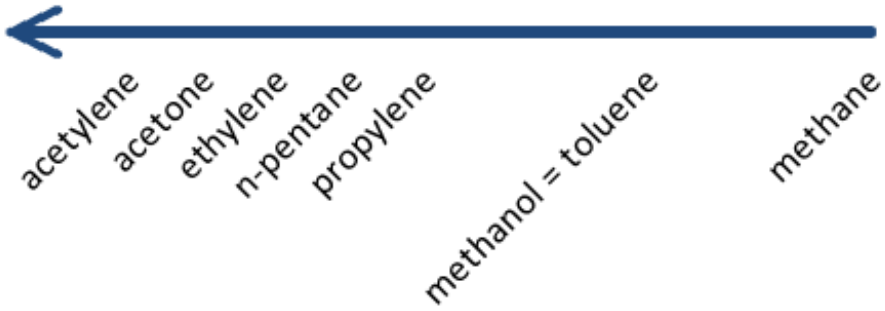

Figure 6: Reactivity orders of various carbon sources for CNT synthesis

There are different carbon nanotube formation mechanisms proposed in the experimental literature. According to Yu and coworkers, carbon nanotube formation mechanism starts with the decomposition of gaseous carbon source on the metal catalyst. Then carbon atoms, coming from the carbon source, diffuse into the metal bulk. Finally precipitating carbons form carbon nanotube. Kim and Sigmund also proposed the same mechanism. However, they stated that the form of catalyst was not clear during the process. According to their study, catalyst may be in pure metallic carbide or pure metal during the reactions. Another mechanism was proposed by Helveg et al., in the work of Yu and coworkers, as the decomposition of carbon source on the metal surface, surface diffusion of carbons and nucleation of carbon nanotube (Kim & Sigmund, 2005; Yu, et al., 2005). Li and coworkers proposed similar mechanism

including carbon cluster formation and their dissolution in the metal bulk followed by the formation of carbon nanotubes from the carbon precipitate (Li, et. al., 2010). According to Ni and coworkers, catalyst particles help dissociation of carbon source during the carbon nanotube synthesis process. They propose that carbons of decomposed carbon source generate metal carbide with the catalyst used. Then this carbide decomposes after a certain temperature and creates carbon nanotubes (Ni, et. al., 2009).

Although there are some proposed mechanisms, elementary steps of carbon nanotube production are not exactly determined yet, especially for catalytic surface reactions. Also physical state and the chemical composition of the catalyst particles are still mysterious for the mechanisms (Kim & Sigmund, 2005). However, according to the results of the kinetic studies conducted for methane as carbon source, rate determining step was found as the dissociation of the carbon source (Ni, et al., 2006; Pirard, et. al., 2007).

CHAPTER 3

COMPUTATIONAL METHODOLOGY AND SURFACE MODELS

Computations in this study were started with the construction of bulk structures of metals (Fe and Ni) from the lattice data obtained in the literature. Then constructed bulk structures were optimized by using Vienna Ab-initio Simulation Package (VASP) code (sample VASP input files can be seen in Appendix A). Afterwards, optimized bulk structures were cleaved to get desired surfaces (Fe(111), Ni(100) and Ni(111)) with appropriate depth. Then, these cleaved surfaces were optimized again. Final optimized surfaces were used for the acetylene adsorption and dehydrogenation steps. First, acetylene adsorption was studied on the surface. Up to this point everything was clear with the mechanism. However following step was the dehydrogenation of acetylene, and the exact mechanism was unknown. Because of this reason three possible mechanisms were tried to remove hydrogens of acetylene from the system. For the first mechanism one of the hydrogens was sent to other hydrogen and obtained hydrogen molecule desorbed to the gas phase. For the second mechanism, hydrogens of adsorbed acetylene were desorbed to gas phase one by one. Finally, for the third mechanism hydrogens of adsorbed acetylene were sent to the metal surface one by one. Then, one of the surface hydrogens was sent to other hydrogen atom to form hydrogen molecule and hydrogen molecule was desorbed to the gas phase. To be able to find transition state geometries, climbing image nudged elastic band (CI-NEB)

calculations were conducted for all steps (except adsorption and desorption). Results of the CI-NEB calculations were followed by transition state geometry and vibrational frequency calculations.

Energetics of the mechanisms was calculated by using equation (26) for all steps.

$$E_{rxn} = E_{products} - E_{reactants} \quad (26)$$

For the adsorption step reactants were taken as optimized surface and gas phase acetylene. Product of the adsorption step was the surface with adsorbed acetylene. For other steps of the mechanisms, reactant was taken as the initial structure and the product is the final structure studied. Activation barriers were calculated by using CI-NEB calculation results. Finally, relative energy versus reaction step diagrams were plotted for all paths.

3.1. Vienna Ab-initio Simulation Package (VASP) Code

Vienna Ab-initio Simulation Package (VASP) was used for all quantum mechanical calculations to simulate surface carbon obtaining procedure in this thesis. VASP code was developed in University of Vienna by George Kresse, Jungen Furthmuller and their team (Kresse & Furthmuller, 1996; Kresse & Hafner , 1994). Software uses density functional theory (DFT) to be able to get information about the systems of interest. Code treats given finite unit cell like an infinite (periodic) system and solves Kohn Sham equations by taking into that periodic cell. Figure 7 shows the unit cell of Fe(111) slab and its equivalent structure during calculations with VASP code. Vienna Ab-initio Simulation Package code uses plane wave basis set and pseudo potentials for quantum mechanical solution process and includes two loops. One of these loops is responsible for the calculation of the energies and forces and the second loop is responsible for the

ionic movements for the optimization of the geometries. Code used in this thesis work also includes projector augmented wave (PAW) method and generalized gradient (GGA) approximations with the usage of supercell approach. PAW method was used for electron ion interactions in the system and generalized gradient approximation was used for the explanation of the exchange correlation term in the Kohn Sham equation (Blöchl, 1994; Perdew, et al., 1992).

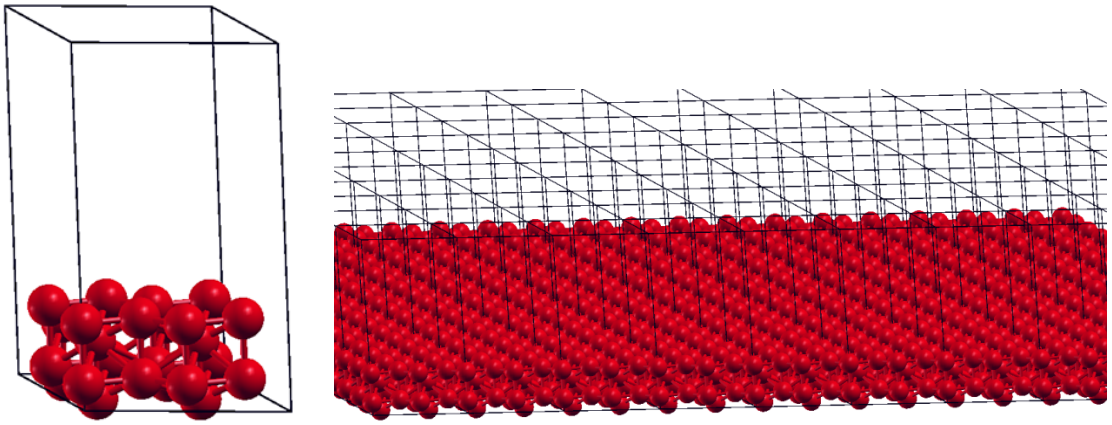

a b

Figure 7: a) Fe(111) 3x3 unit cell b) infinitely representation of Fe(111) unitcell in x and y directions as VASP threat the unitcell in a

During simulations, equilibrium structures of reactants and products were obtained by using standard VASP code. However, to be able to find transition states standard technique was not sufficient. Reaction coordinate between products and reactants were studied by climbing image nudged elastic band (CI-NEB) method and transition states were determined according to CI-NEB and vibrational frequency calculations. Additionally, Climbing Image method was implemented to the NEB calculations for the accuracy. NEB generates intermediate images between reactants and products and optimizes them to find reaction pathway. This optimization code relaxes each

intermediate image separately by considering spring forces between the images. With the implementation of CI method, true force was taking into account instead of string force (Institute for Theoretical Chemistry, University of Texas at Austin).

3.2. Fe (111) Surface

Iron bulk has a body centered cubic (bcc) structure with space group Im-3m and space group number of 229. Each sides of the cubic structure have a length of 2.867Å (Winter, Iron: crystal structure, 2010). After the relaxation, lattice parameters of the structure were found to be 2.757Å. Representation of the relaxed crystal structure of Fe bulk structure can be seen in Figure 8.

After the bulk structure of iron was prepared, (111) surface was cleaved with the depth of five layers. Then 2x2 supercell was created by using cleaved structure. Finally, 10Å vacuum region was inserted at the top of the slab prepared. This prepared structure was optimized one more time to be able to get final optimized Fe(111) slab. Optimized Fe(111) slab can be seen in Figure 10 at the end of the chapter.

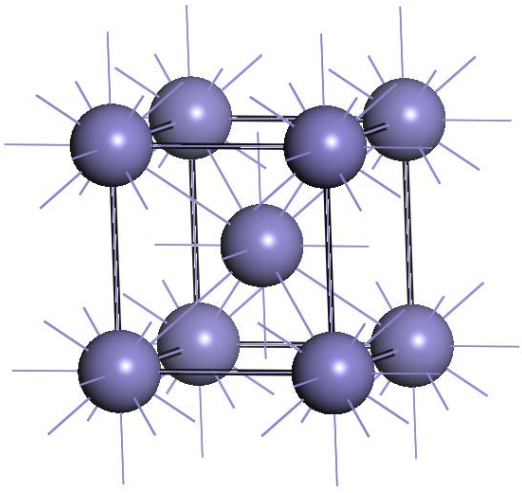

Figure 8: Representation of optimized crystal structure of Fe bulk

3.3. Ni (100) and Ni(111) Surfaces

Preparation of Ni(100) and Ni(111) surfaces were started with the same step, construction and relaxation of bulk structure. Nickel bulk has face centered cubic structure (fcc) with side lengths of 3.524Å (Winter, Nickel: crystal structure, 2010). After the relaxation process this value was found to be 3.516Å. Relaxed nickel bulk structure can be seen in Figure 9.

Ni(111) surface was cleaved from the bulk structure with the depth of 3 layer. By using cleaved structure 3x3 supercell was created and 10Å thick vacuum region was added to the surface. After further optimizations Ni(111) surface became ready for the study. Optimized Ni(111) structure can be seen in Figure 10.

Ni(100) surface was again cleaved from the relaxed bulk structure of nickel with the depth of 1.5. By using cleaved structure 3x3 supercell was created. 10Å vacuum region was again added to the top of the surface as it was done for the other two surfaces. Then prepared structure was optimized with VASP code to finalize the optimized geometry of Ni(100) surface. Optimized Ni(100) structure can be seen in Figure 10.

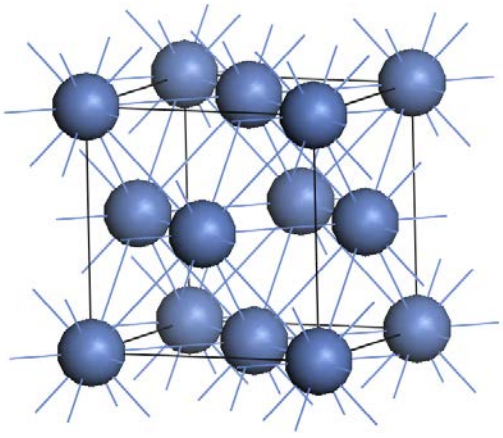

Figure 9: Representation of optimized crystal structure of Ni bulk

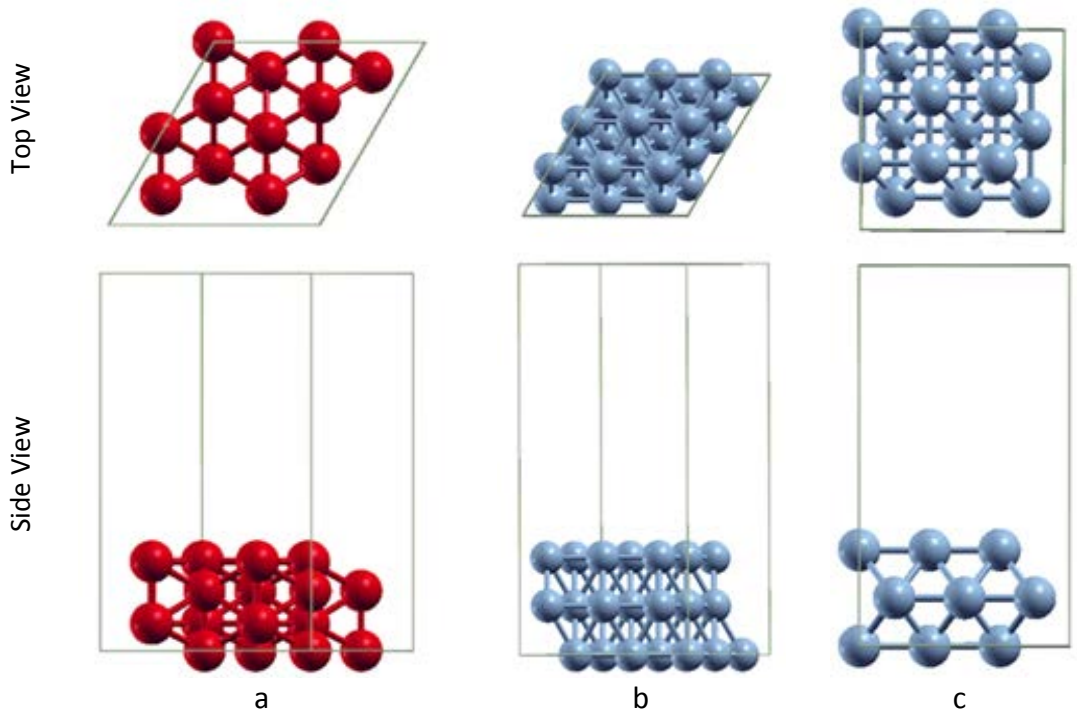

Figure 10: Optimized structures of surfaces a) Fe(111) b) Ni(111) c)Ni(100)

CHAPTER 4

RESULTS AND DISCUSSION

Main part of the study started after the preparation of the metal surfaces, which was explained in previous chapter. The procedure followed for each surface after the surfaces were ready can be divided into two parts. First, acetylene was adsorbed to the surface of interest and acetylene-surface complex structure was obtained. Then acetylene was dehydrogenated and surface carbons were obtained. For all metal surfaces, work to do was very clear up to dehydration part. Bulk relaxation, surface preparation and acetylene adsorption steps were the simple part of the study. The main challenge was finding the mechanism with minimum activation barriers for the surface carbon formation. For this aim three different mechanisms were studied for all surfaces. These mechanisms were named as:

Method I: Direct hydrogen-hydrogen interaction method

Method II: Hydrogen atom desorption method

Method III: Surface-hydrogen interaction method

These methods will be explained in more detail with their result for Fe(111), Ni(100) and Ni(111) slabs below.

4.1. Quantum Mechanical Calculations for Fe(111) slab

As it is stated above, quantum mechanical calculations for the surface nanocarbon production pathway were started with the adsorption of acetylene on the optimized Fe(111) surface. According to calculations conducted, energy for the adsorption of acetylene to the Fe(111) surface were found as -2.8eV. At the end of the computations, geometry in the Figure 11 was obtained.

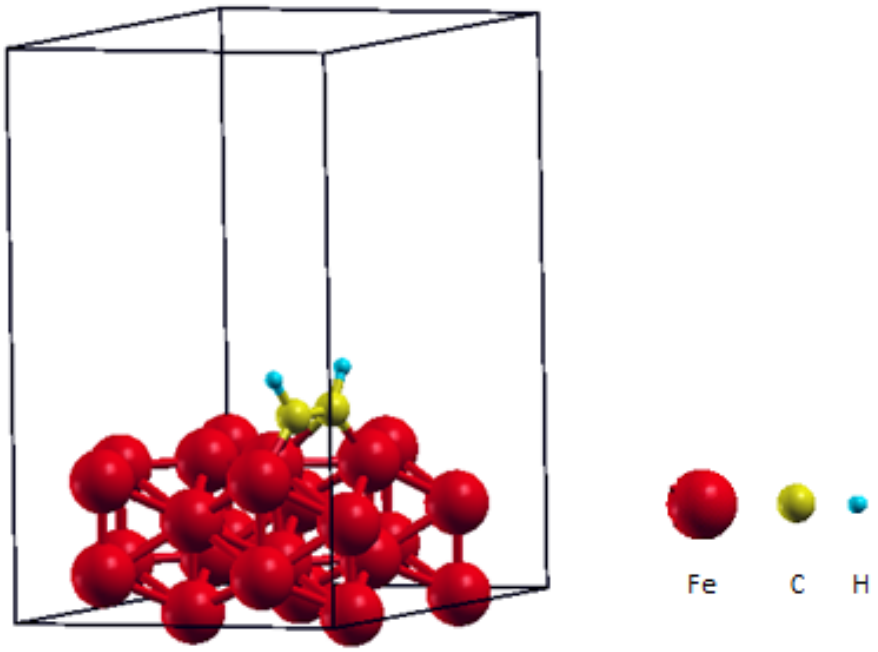

Figure 11: Surface-acetylene complex obtained for Fe(111) slab

After the surface-acetylene complex was obtained, direct hydrogen-hydrogen interaction, hydrogen atom desorption and surface-hydrogen interaction methods were studied and their results were compared. Additionally, behavior of the slab for additional acetylene adsorptions were studied separately and attached as Appendix B.

4.1.1. Direct Hydrogen-Hydrogen Interaction Method for Fe(111) Slab

For direct hydrogen-hydrogen interaction method, hydrogens of acetylene molecule were directly interacted and produced hydrogen molecule was desorbed to the gas phase. For this aim one of the hydrogen atoms was sent to the other one. Diagram of this mechanism can be seen in Figure 12. After the final geometry was obtained, CI-NEB calculations were conducted between initial (geometry surface-acetylene complex) and final (geometry after hydrogen molecule desorbed togas phase) geometries. By using the results of CI-NEB calculations with the results of transition state and vibrational frequency calculations, activation barrier of the reaction was found as 3.6eV. Figure 13 shows relative energy profile for this method. In the figure, R represents reference state of the system, which is the gas phase acetylene plus Fe(111) surface, A represents the surface-acetylene complex obtained with adsorption, TS represents the transition state and F represents the final state of the system. Final state includes Fe(111) slab with surface carbons and hydrogen molecule in gas phase. Final structure can be seen in Figure 14.

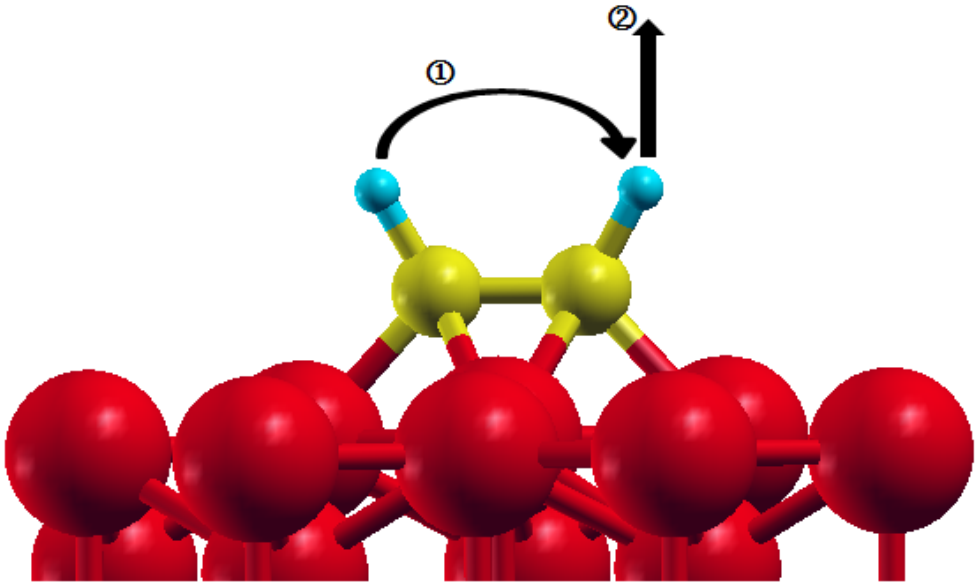

Figure 12: Digram of direct hydrogen-hydrogen interaction method

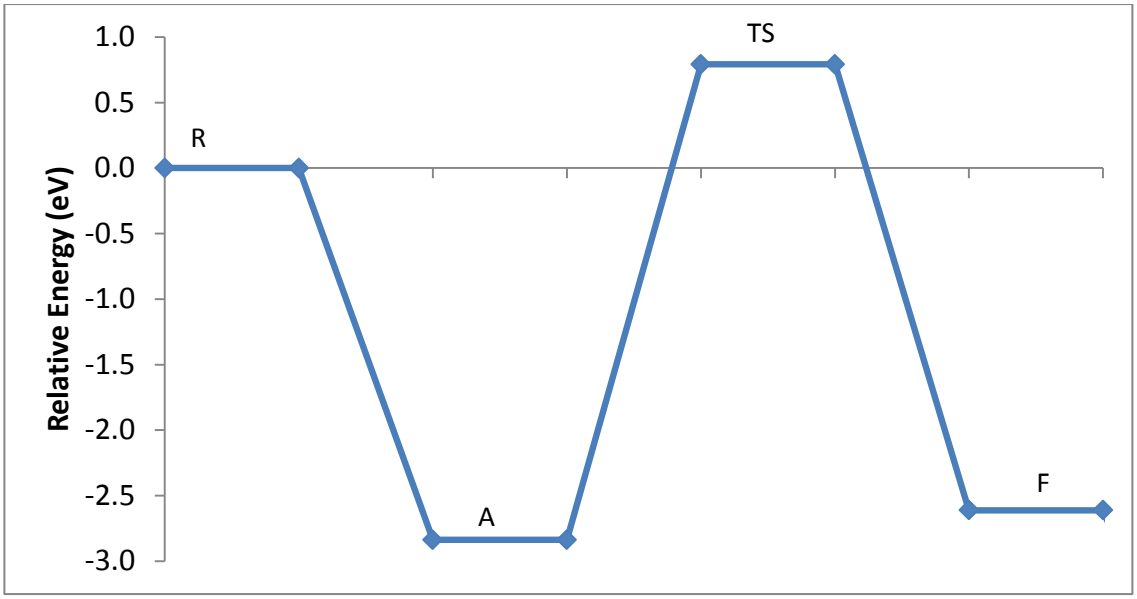

Figure 13: Relative energy plot for the steps of direct hydrogen-hydrogen interaction method for Fe(111) slab

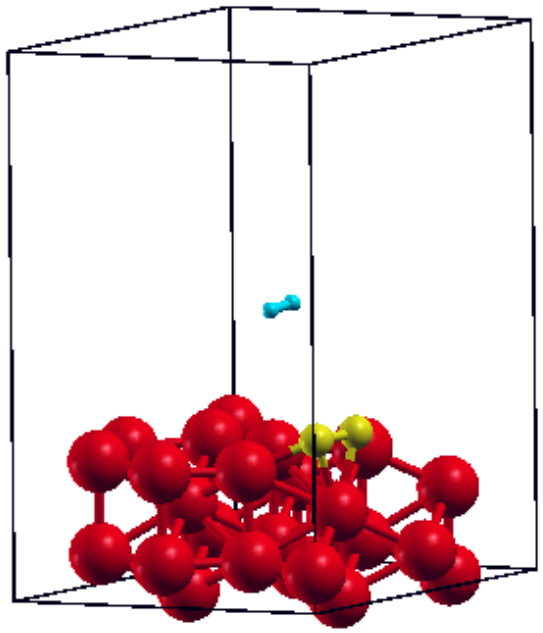

Figure 14: Final structure obtained at the end of direct hydrogen-hydrogen interaction method for Fe(111) slab

4.1.2. Hydrogen Atom Desorption Method for Fe(111) Slab

For hydrogen atom desorption method, hydrogen atoms were desorbed to the gas phase one by one and surface carbons were obtained at the end of the process. Diagram showing this process was given in Figure 15. Hydrogen atoms that were desorbed to gas phase were assumed to interact in the gas phase. For this mechanism, energy required to desorb the first hydrogen was found as 3.4eV and the energy required to desorb the second hydrogen to the gas phase was found as 3.6eV. Relative energy profile of hydrogen atom desorption method can be seen in Figure 16. In the figure H1 represents the energy level for desorption of first hydrogen and H2 represents the energy level for desorption of the second hydrogen.

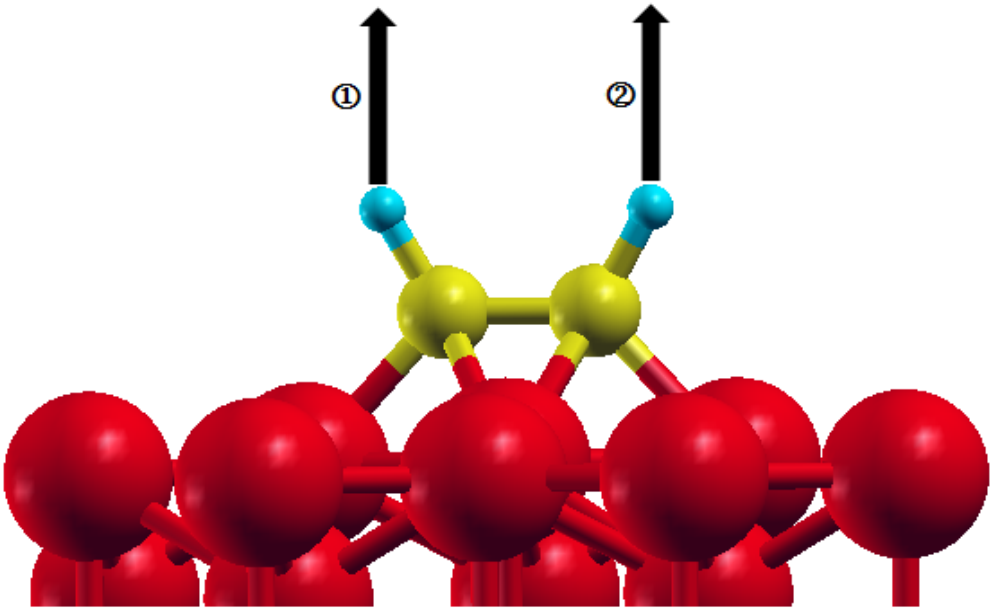

Figure 15: Digram of direct hydrogen-hydrogen interaction method

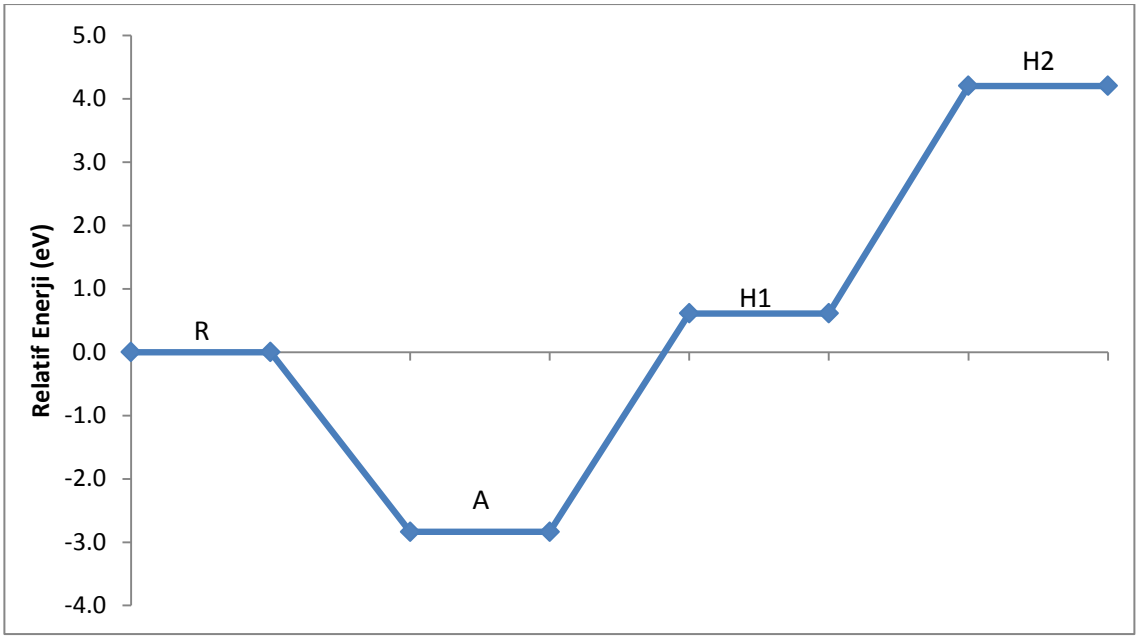

Figure 16: Relative energy plot for the steps of hydrogen atom desorption method for Fe(111) slab

4.1.3. Surface-Hydrogen Interaction Method for Fe(111) Slab

For surface-hydrogen interaction method, hydrogens of acetylene were interacted with the metal surface one by one. Hydrogen atoms on the metal surface were interacted with surface diffusion and created hydrogen molecule and this hydrogen molecule was desorbed from the surface. In the Figure 17, diagram of this process was given. According to CI-NEB and TS state calculations activation barrier for the interaction of first hydrogen of the acetylene with Fe(111) surface was found as 0.7eV, and activation barrier for the interaction of the second hydrogen atom with the Fe(111) surface was found as 0.7eV again. Relative energy profile of surface-hydrogen interaction method can be seen in Figure 18. In the figure TS1 and TS2 represent level of transition state geometries and Fe-H1 and Fe-H2 represent the final level of the surface-hydrogen interaction for the numbered hydrogen. H1-H2 represents the final state after surface

hydrogens were interacted with surface diffusion and desorbed to gas phase as hydrogen molecule.

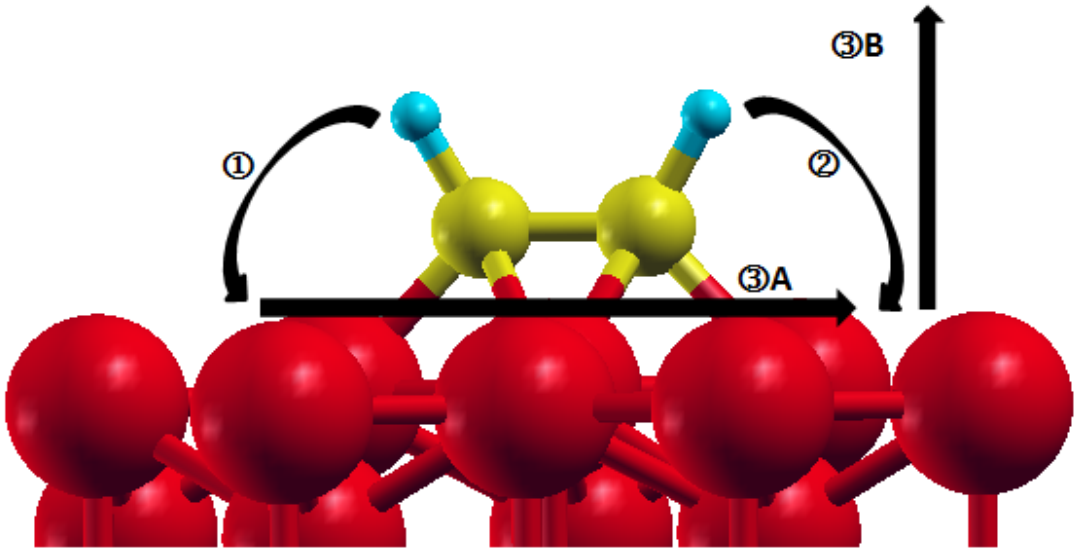

Figure 17: Digram of direct hydrogen-hydrogen interaction method

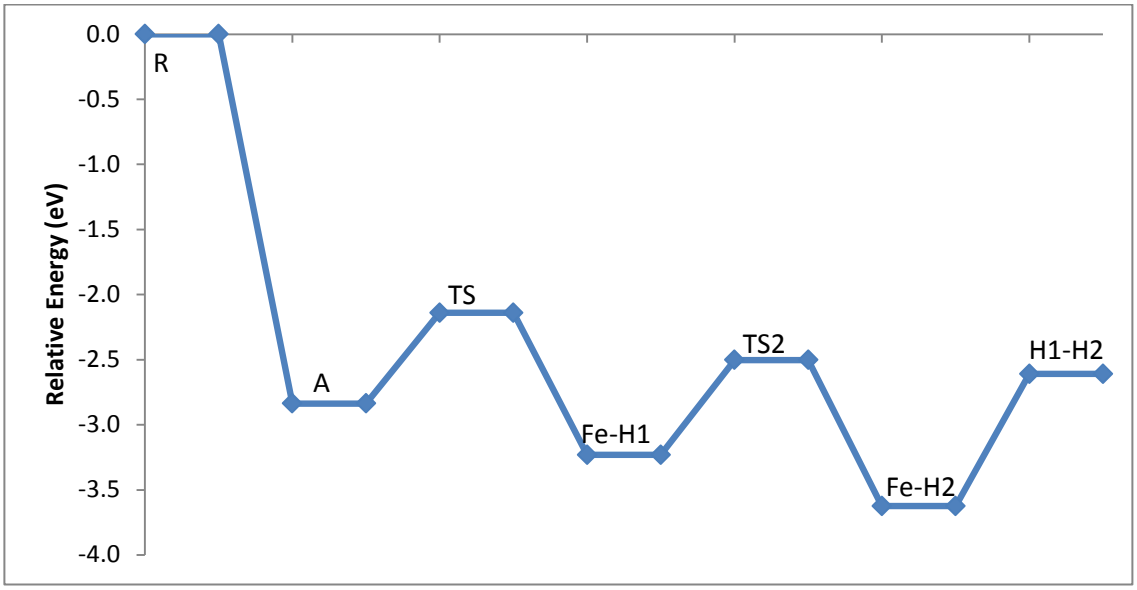

Figure 18: Relative energy plot for the steps of surface-hydrogen interaction method for Fe(111) slab

4.1.4. Comparison of the Methods Studied for Fe(111) Slab

Numerical values of activation barriers and desorption energies were given above. However, to be able to make a comparison, it can be better to collect all three methods studied for Fe(111) surface into one graph. Figure 19 shows relative energy levels of all three mechanisms studied for Fe(111) slab. As it can be clearly seen from Figure 19, surface-hydrogen interaction method leads lower activation barriers and gives best pathway among the methods studied. This result was thought to be achieved due to better interaction of hydrogen atoms with the catalyst surface. By surface-hydrogen interaction mechanism, catalyst showed its promoter effect better.

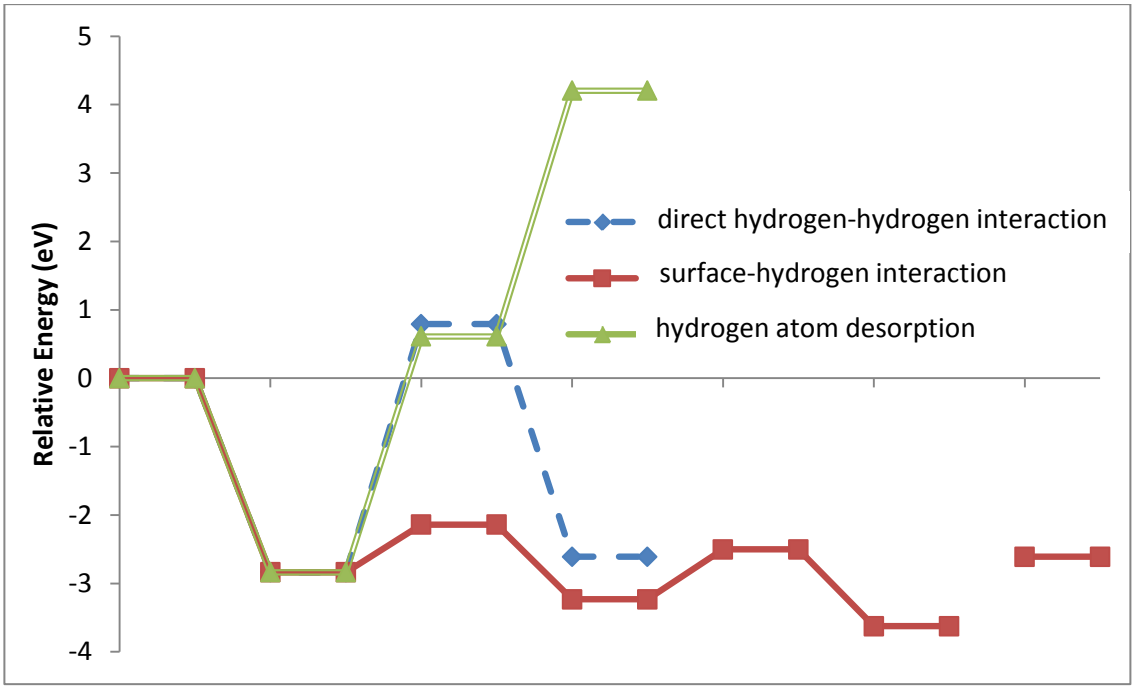

Figure 19: Relative energy levels of all three mechanisms studied for Fe(111) slab

4.2. Quantum Mechanical Calculations for Ni(100) slab

Optimized Ni(100) slab was first used for the adsorption of acetylene. With this step, surface-acetylene complex was obtained. Acetylene surface complex structure may be seen in Figure 20. For this process relative energy value was found as -2.9eV.

After the surface acetylene complex was obtained for the Ni(100) slab, direct hydrogen-hydrogen interaction, hydrogen atom desorption and surface-hydrogen interaction methods were studied again as it was done for Fe(111) slab.

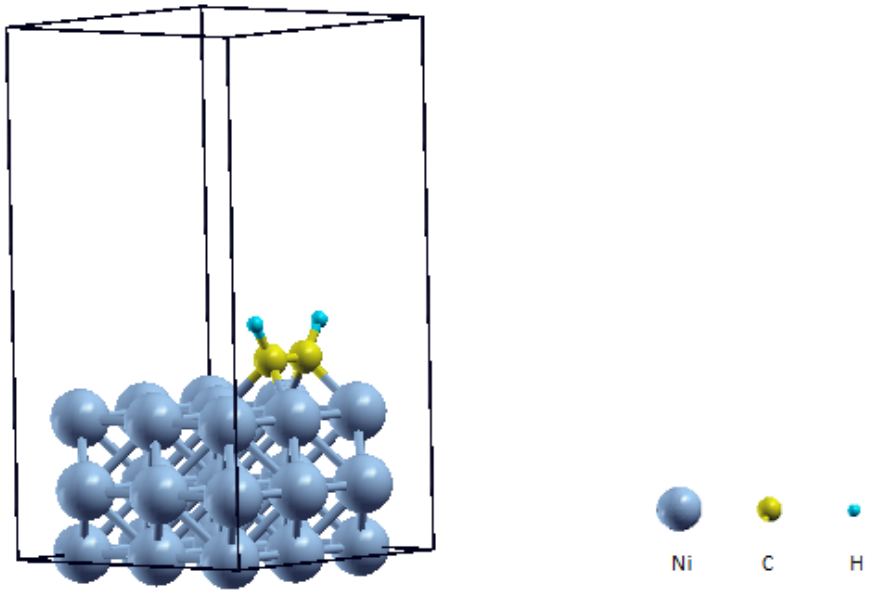

Figure 20: Surface-acetylene complex obtained for Ni(100) slab

4.2.1. Direct Hydrogen-Hydrogen Interaction Method for Ni(100) Slab

Structure for the study of surface carbon production was ready after the adsorption of acetylene. First direct hydrogen-hydrogen interaction method was studied for Ni(100) slab like it was done for the other slabs. One of the hydrogen molecules was sent to the

other one and hydrogen molecule was formed. Produced hydrogen molecule desorbed to the gas phase as a part of interaction and slab remained with the carbons of acetylene. Relative energy of the final structure was found to be 2.15eV. Before starting the time consuming CI-NEB calculations (takes approximately 1 month) for this step, it was decided to investigate the results of the other two methods first. When the results were reviewed, it was decided to cancel CI-NEB calculations for this step. Because CI-NEB results will give an activation barrier which was greater or equal to the final energy level and other methods already showed lower activation barriers then the final energy level of this process. Relative energy profile of the direct hydrogen-hydrogen interaction method is given in Figure 21. Also final geometry obtained at the end of the mechanism is given in Figure 22. In Figure 21, R represents reference state including Ni(100) slab and gas phase acetylene, A represents the surface-acetylene complex and F represents final geometry obtained at the end of the procedure.

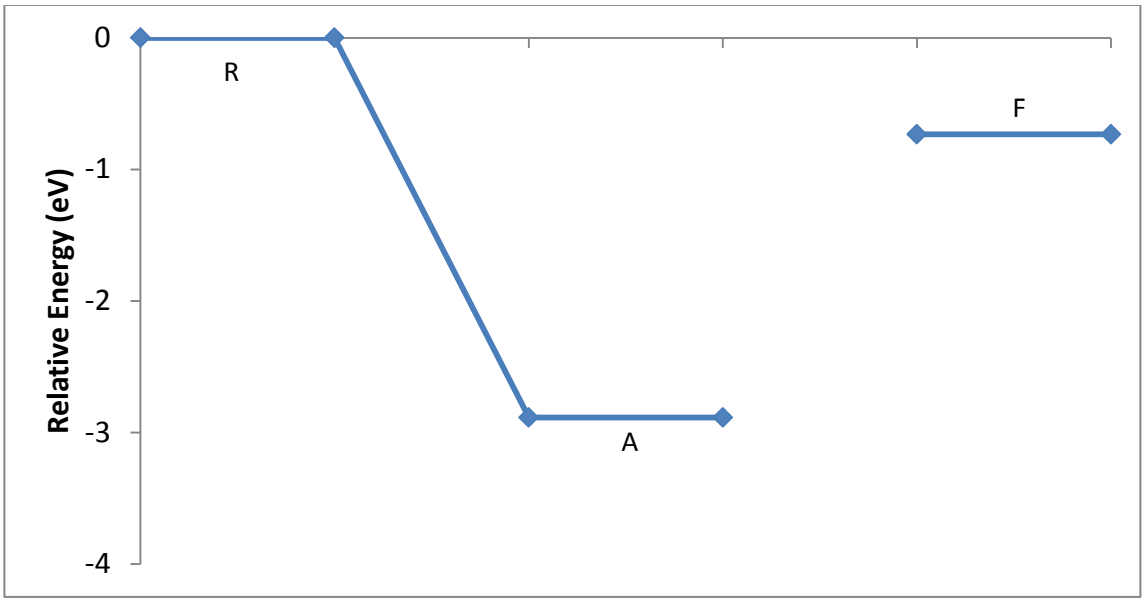

Figure 21: Relative energy plot for the steps of direct hydrogen-hydrogen interaction method for Ni(111) slab

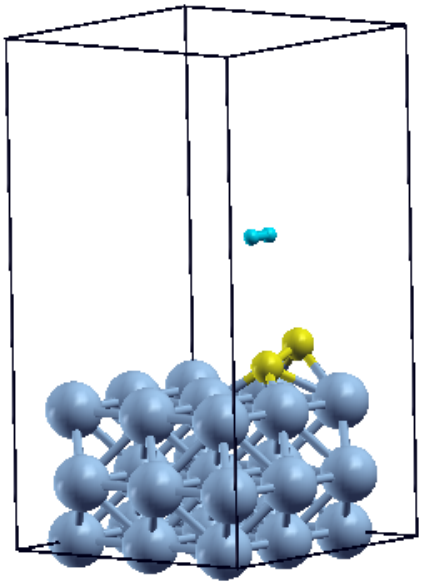

Figure 22: Final structure obtained at the end of direct hydrogen-hydrogen interaction method for Ni(100) slab

4.2.2. Hydrogen Atom Desorption Method for Ni(100) Slab

Second method used for the surface carbon production on Ni(100) slab was hydrogen atom desorption method. For this aim, hydrogens, coming from the adsorbed acetylene, were desorbed to the gas phase one by one. Energy value required to desorb first hydrogen to the gas phase was found as 3.8eV from the quantum mechanical calculation results. Energy required for desorption of second hydrogen was found as 5eV. Relative energy profile of this mechanism can be seen in Figure 23. Plot starts again with the reference state R, A represents the state of the system after acetylene adsorption and H1 and H2 represent desorption of the hydrogen atom whose number was stated next to it.

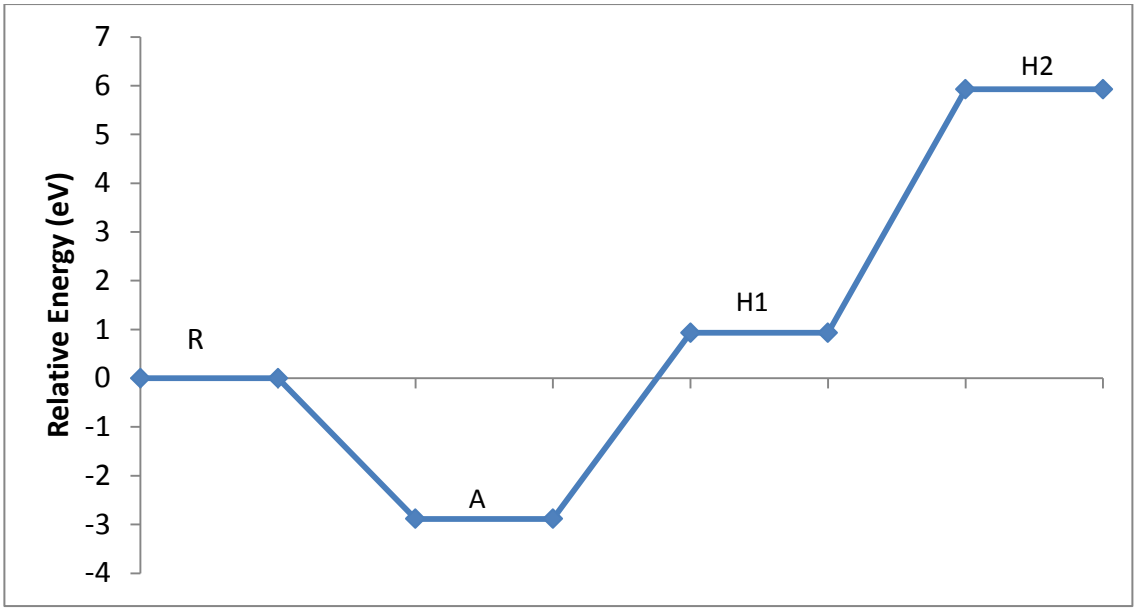

Figure 23: Relative energy plot for the steps of hydrogen atom desorption method for Ni(100) slab

4.2.3. Surface-Hydrogen Interaction Method for Ni(100) Slab

As the third mechanism, surface-hydrogen interaction method was studied for the Ni(100) slab. Hydrogen atoms of adsorbed acetylene were sent to metal surface one by one. After the completion of this process surface hydrogens were diffused to give hydrogen molecule. Produced hydrogen molecule was desorbed as a part of this mechanism step. According to quantum mechanical calculation results, activation barrier for the interaction of first hydrogen with the Ni(100) surface was found as 0.8eV as a result of CI-NEB and transition state calculations. Activation barrier for the interaction between second hydrogen and the Ni(100) surface was found to be 1.6eV. Also activation barrier for the hydrogen molecule formation and desorption step was found as 1.1eV. Relative energy profile of the surface-hydrogen interaction method for Ni(100) slab is given in Figure 24. In the plot, R represents reference state and A represents surface-acetylene complex which was formed by the adsorption of

acetylene. Ni-H1 and Ni-H2 represent the final structure after the hydrogen with given number was adsorbed on the surface. TS1 and TS2 represent the transition states of these steps. H1-H2 is the structure after hydrogen gas was desorbed to gas phase and TS3 represents the transition state for the step.

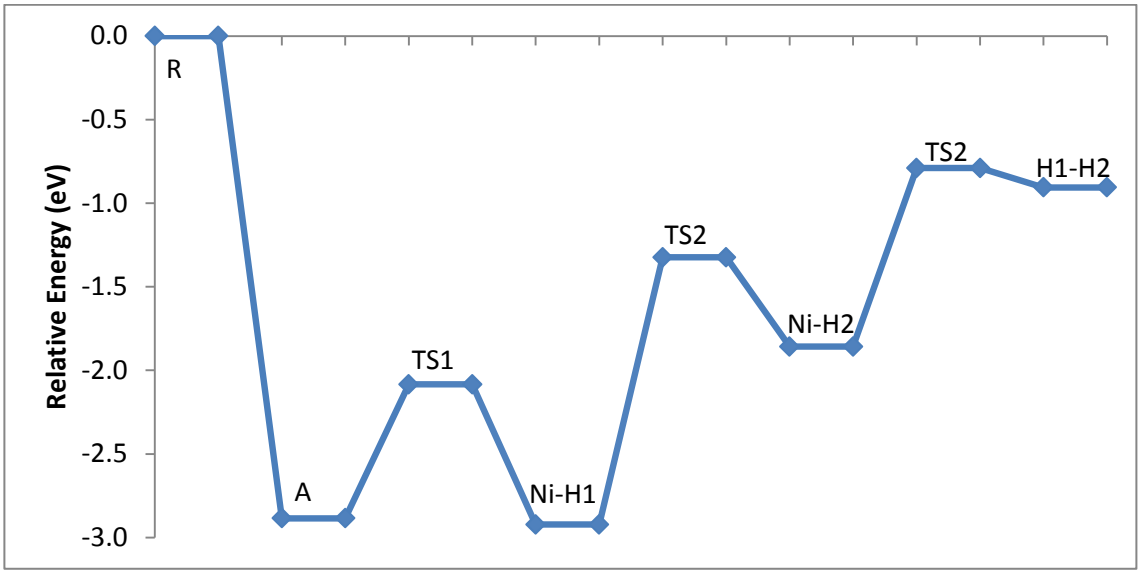

Figure 24: Relative energy plot for the steps of surface-hydrogen interaction method for Ni(100) slab

4.2.4. Comparison of the Methods Studied for Ni (100) Slab

In order to be able to make a good comparison between the three mechanisms studied for Ni(100) slab, Figure 25 is plotted to show results of all three pathways. As it can be seen from the Figure 25, surface-hydrogen interaction method gives the most possible pathway among the methods studied. Again it was thought that the effect of catalyst surface was shown in the surface hydrogen interaction method better than the other two methods. This catalytic effect leads lower activation barriers for the steps.

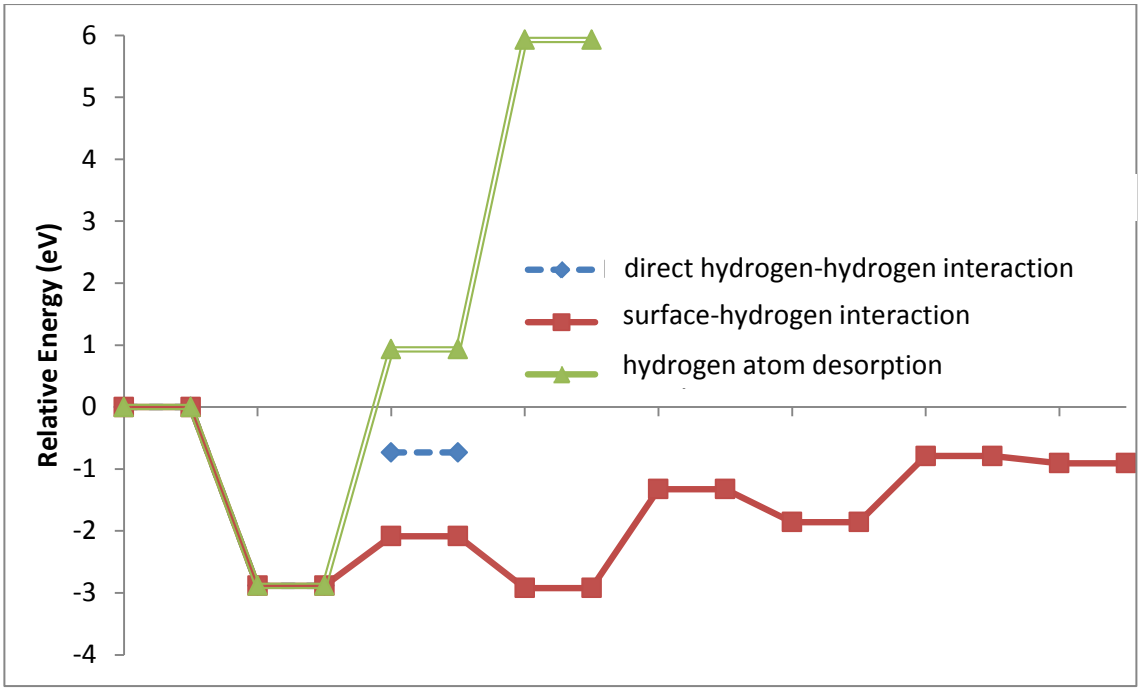

Figure 25: Relative energy levels of all three mechanisms studied for Ni(100) slab

4.3. Quantum Mechanical Calculations for Ni(111) slab

Like the studies conducted with other surfaces, studies on the Ni(111) slab was started with the adsorption of acetylene on the optimized Ni(111) surface and surface-acetylene complex was obtained. Relative energy of this step was found as -3.5eV according to results of quantum mechanical calculations. At the end of these quantum mechanical calculations, structure in the Figure 26 was obtained.

After this step, same three mechanisms with the Fe(111) and Ni(100) were studied for Ni(111) again. Performances of these three methods were also compared for Ni(111) slab. For the letter representations in the figures, exactly same nomenclature in Ni(100) section is used.

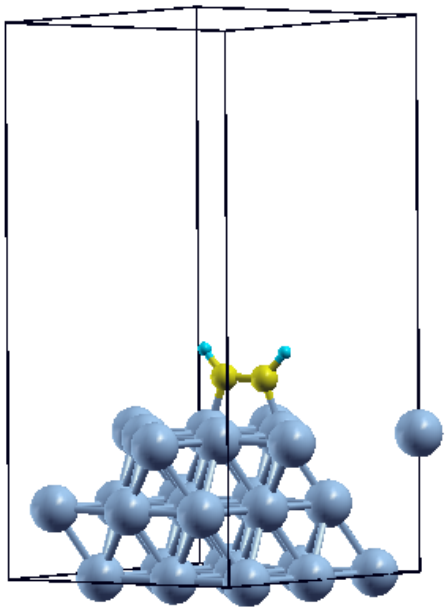

Figure 26: Surface-acetylene complex obtained for Ni(111) slab

4.3.1. Direct Hydrogen-Hydrogen Interaction Method for Ni(111) Slab

Procedure was again the same with the direct hydrogen-hydrogen interaction method used for other slabs. Hydrogen atoms of the acetylene adsorbed on the Ni(111) surface was interacted and produced hydrogen molecule was desorbed to the gas phase. According to results of the quantum mechanical calculations, relative energy of the final geometry was found to be 2.7eV and activation barrier equal to at least this value (probably it is higher) should be overcome in order to conduct this step. Because of the results of the other two methods, CI-NEB calculation was not considered to be necessary. Relative energy diagram of the direct hydrogen-hydrogen interaction method for Ni(111) slab is shown in Figure 27 and the final structure of this mechanism is given in Figure 28.

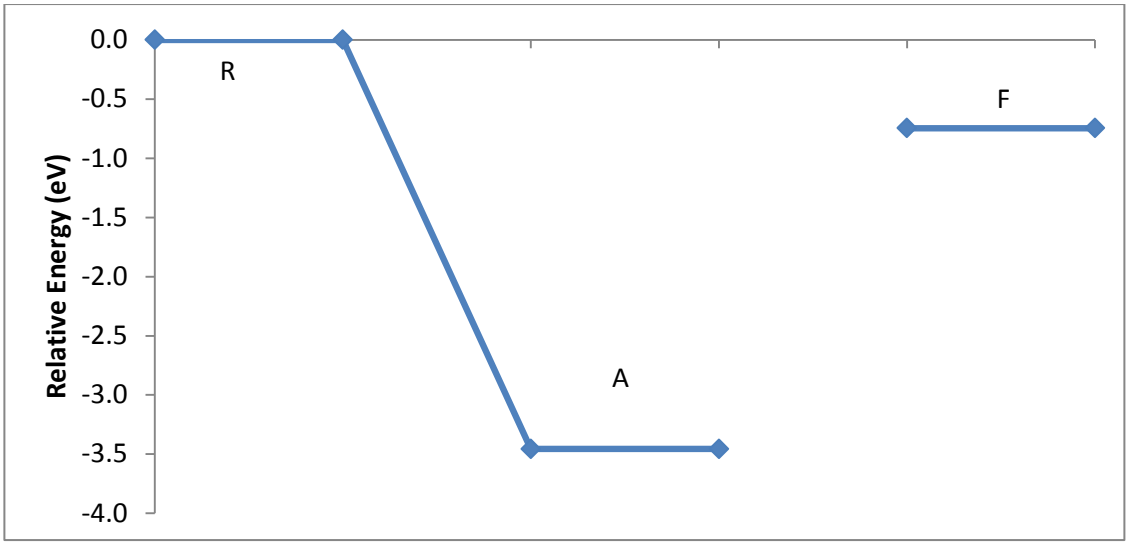

Figure 27: Relative energy plot for the steps of direct hydrogen-hydrogen interaction method for Ni(111) slab

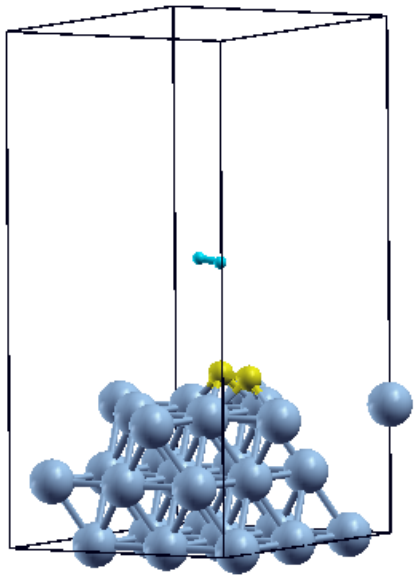

Figure 28: Final structure obtained at the end of direct hydrogen-hydrogen interaction method for Ni(111) slab

4.3.2. Hydrogen Atom Desorption Method for Ni(111) Slab

Order of the studied mechanisms were kept for the Ni(111) and hydrogen atom desorption mechanism was studied as the second mechanism. Hydrogens of adsorbed acetylene were directly desorbed to gas phase one by one. To be able to desorb the first hydrogen, step was required and energy of 4.3eV. This energy for desorption of second hydrogen was found as 5.2eV. Relative energy plot for the mechanism is given in Figure 29.

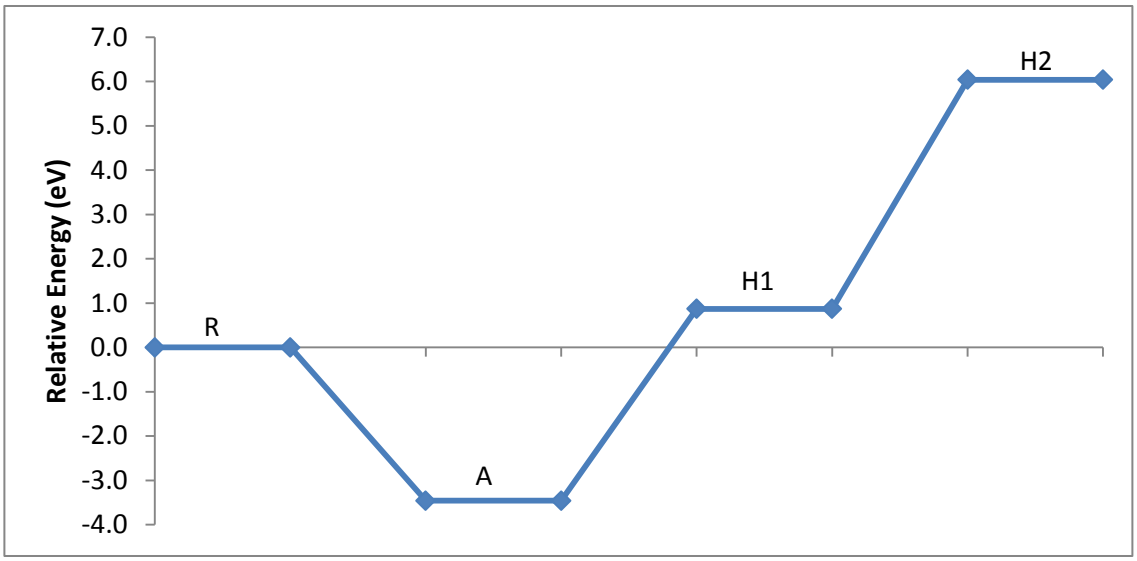

Figure 29: Relative energy plot for the steps of hydrogen atom desorption method for Ni(111) slab

4.3.3. Surface-Hydrogen Interaction Method for Ni(111) Slab

Final method that was studied under the scope of this thesis work was the surface-hydrogen interaction method for Ni(111) slab. For surface-hydrogen interaction method, hydrogens of the acetylene was sent to the Ni(111) surface. Then surface hydrogens were diffused and hydrogen molecule was formed and desorbed from the surface. In order to find the activation barriers of the steps, CI-NEB calculations and

transition state calculations were conducted. As a result calculations, activation barrier for the interaction of Ni(111) surface with the first hydrogen atom was found as 1.2eV. Activation barrier for the interaction of Ni(111) surface with the second hydrogen atom was obtained as 1.8eV. Finally production of hydrogen molecule by the surface diffusion of hydrogen molecules and desorption of produced hydrogen molecule to gas phase was determined as 1.2eV. Relative energy profile of the surface-hydrogen interaction method for Ni(111) surface is given in Figure 30 with the exactly same nomenclature given for the same method of Ni(100) slab.

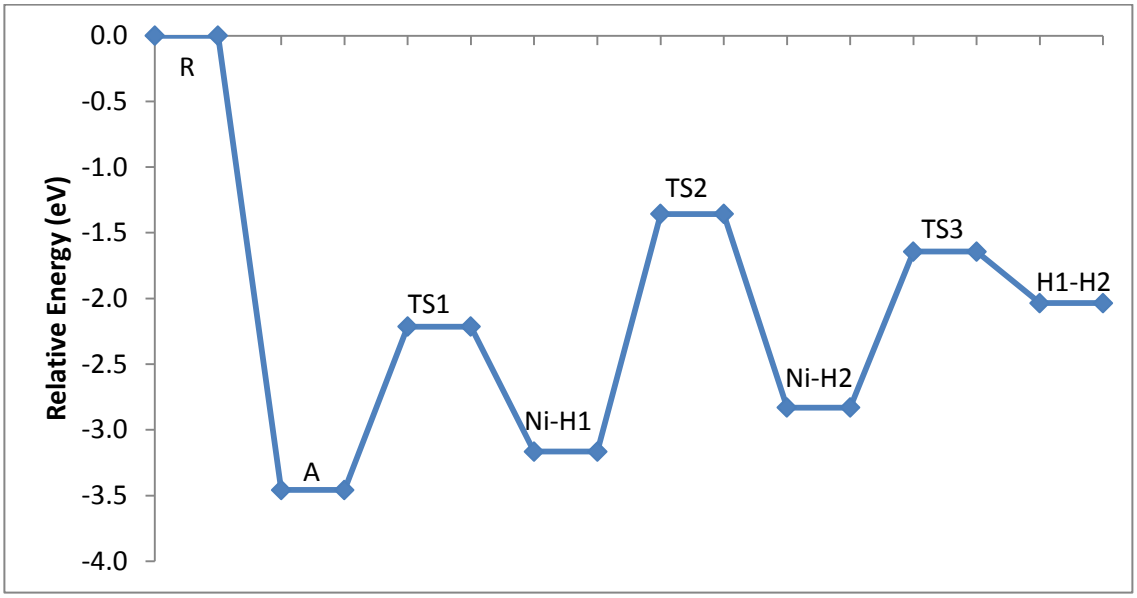

Figure 30: Relative energy plot for the steps of surface-hydrogen interaction method for Ni(111) slab

4.3.4. Comparison of the Methods Studied for Ni (111) Slab

Results obtained from the quantum mechanical calculations of the three mechanism studied for Ni(111) surface are given in Figure 31. As it can be seen in the Figure 31, surface-hydrogen interaction method gives the lowest activation barrier values.

Therefore, it can be said that, the surface-hydrogen interaction method is the most possible pathway for the surface carbon formation on the Ni(111) surface by using acetylene as carbon source. In hydrogen-hydrogen interaction and direct hydrogen desorption mechanisms, catalyst surface only interacted with the carbon atoms. However, in the surface-hydrogen interaction mechanism catalyst particles also showed their effect on the hydrogen atoms. It was thought that this interaction lowered the activation barriers for steps of surface-hydrogen interaction mechanism.

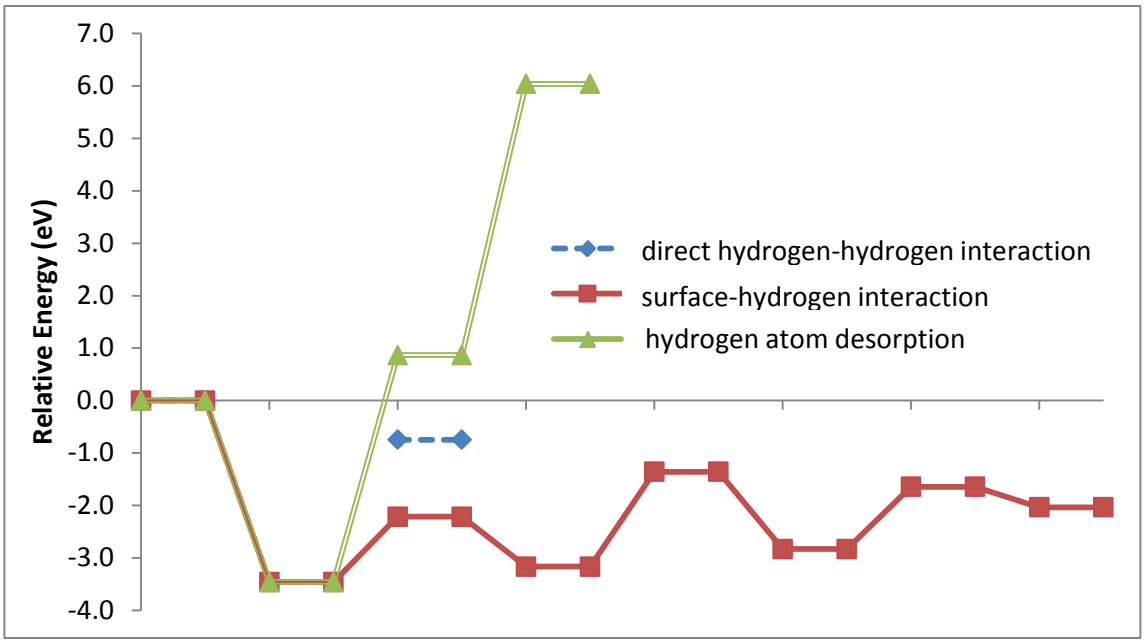

Figure 31: Relative energy levels of all three mechanisms studied for Ni(111) slab

4.4. Comparison of the Performances of the Studied Metal Catalyst Surfaces

Up to this part results of all three mechanisms were given for all metal slabs separately. Also these mechanisms were compared for the individual surfaces and surface-hydrogen interaction method was found to be the most probable pathway for all of the Fe(111), Ni(100) and Ni(111) slabs. In order to make a general comparison between the

slabs used during this study, Figure 32 is plotted for the surface-hydrogen interaction methods of all surfaces. However it was not easy to make a comparison between the performances of the slabs used by using this overall mechanism plot. All activation barriers should be compared step by step for determining the best catalytic surface among these three. Because of this reason, activation barriers of all steps were separately given in Figure 33, Figure 34 and Figure 35.

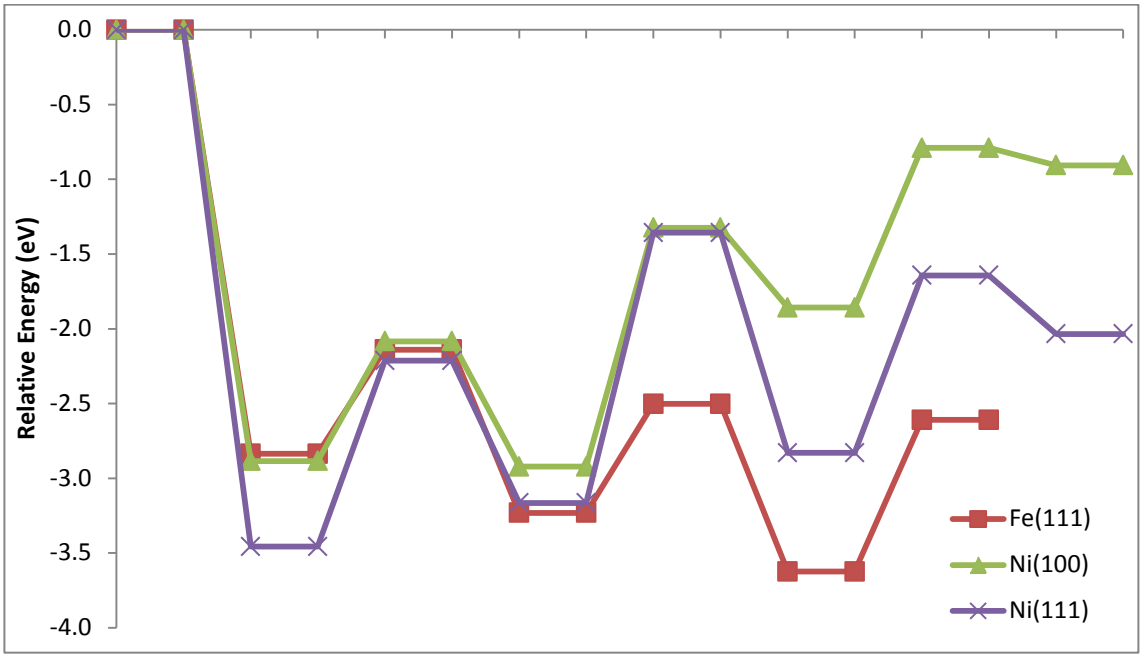

Figure 32: Relative energy levels of surface-hydrogen interaction method for Fe(111),Ni(100) and Ni(111) slabs

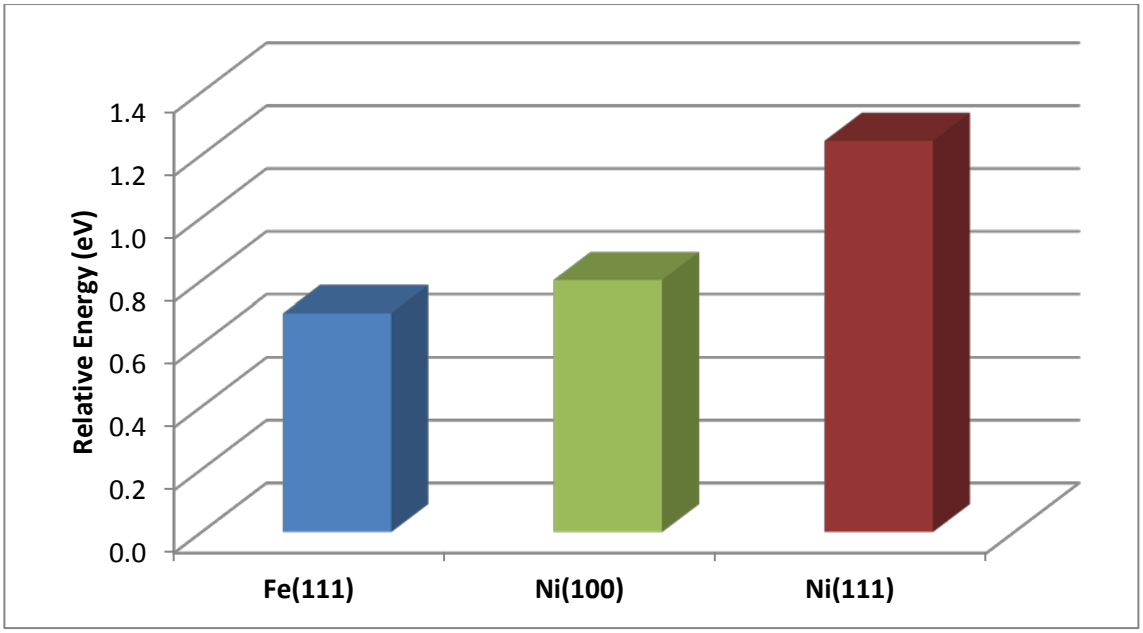

Figure 33: Activation barriers for the interaction of surface with first hydrogen atom for surface-hydrogen interaction mechanism

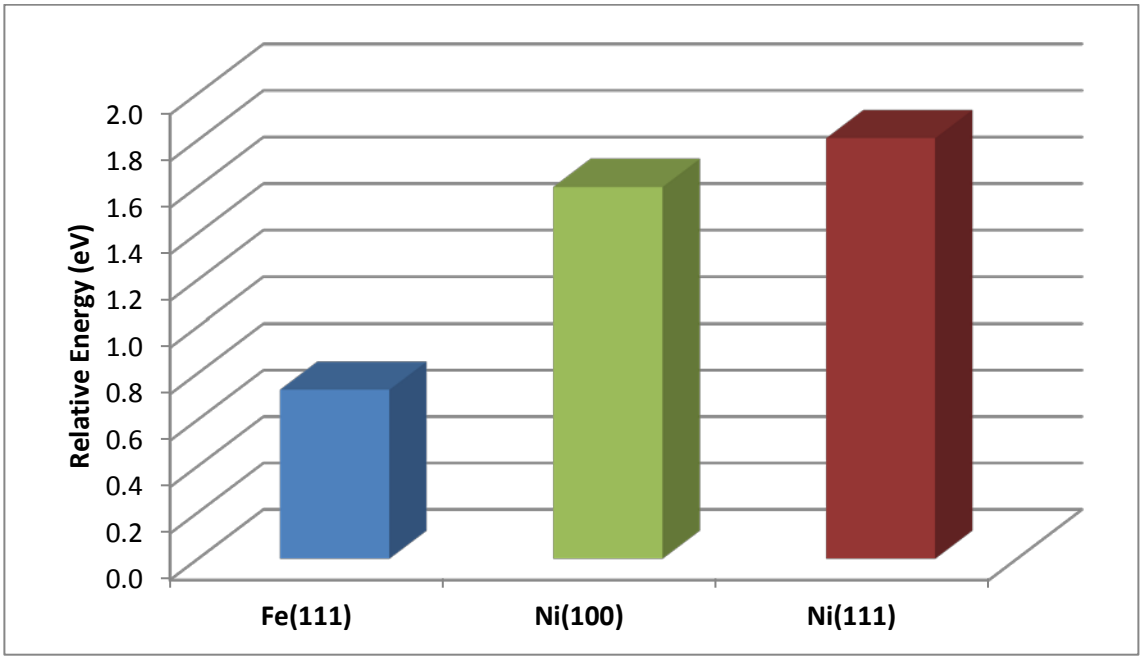

Figure 34: Activation barriers for the interaction of surface with second hydrogen atom for surface-hydrogen interaction mechanism

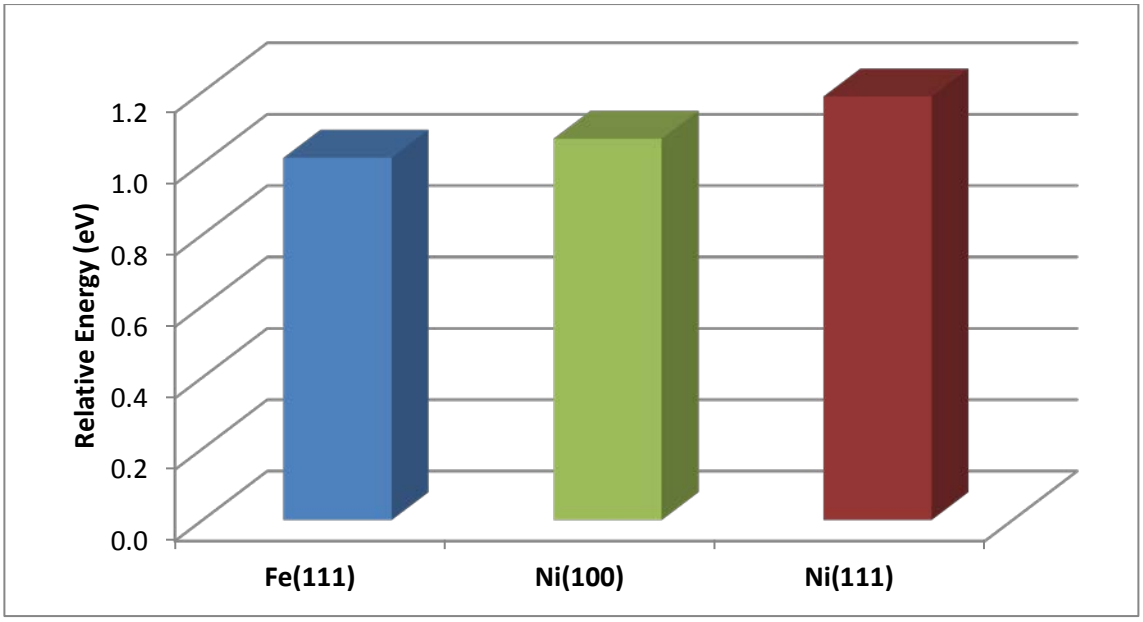

Figure 35: Activation barriers for the interaction of surface hydrogens by diffusion for surface-hydrogen interaction mechanism

When the bar graphs were investigated it can be seen that Fe(111) surface had lowest activation barrier for steps. Because of this reason, reaction can proceed easier on the surface-hydrogen interaction mechanism on Fe(111) slab. In the light of this information, two conclusions were received. First, surface-hydrogen interaction mechanism was the best mechanism among three mechanisms studied. The reason of lower activation barriers obtained with this mechanism was related with the efficient interaction with the catalytic surface. Second, Fe(111) slab shows better catalytical activity than the Ni(100) and Ni(111) slabs.

CHAPTER 5

CONCLUSIONS

Surface nanocarbon formation process was studied throughout this thesis study. Vienna Ab-initio Simulation Package (VASP) code was used to utilize density functional theory (DFT) with generalized gradient approximation (GGA) for all quantum mechanical calculations conducted.

Primary objectives of this study were to compare performances of different metal catalyst surfaces for surface nanocarbon formation and to reveal the most probable mechanism for the surface nanocarbon formation process. In order to achieve these objectives, Fe(111), Ni(100) and Ni(111) surfaces were selected and cleaved from the optimized bulk structures of Fe and Ni metals. These surfaces were used for the surface nanocarbon formation from acetylene by the adsorption and dehydrogenation mechanisms. Adsorption of acetylene to the metal surface was studied as the first step of the mechanism. Second step was the dehydrogenation of acetylene on the surface. However, it was required to find most probable mechanism for the dehydrogenation of acetylene. This necessity was fulfilled by the investigation of three mechanisms for this process. According to the results of this mechanistic study, surface-hydrogen interaction mechanism was found to have lowest activation barriers for all three surfaces. In the light of these results, surface carbon formation mechanism was found to be composed of three steps including acetylene adsorption to the metal catalyst

surface. First step was the acetylene adsorption to the metal surface. Second one was the one by one interaction of hydrogens with the metal surface. Final step was the formation of hydrogen molecule from surface hydrogen atoms and its desorption.

After the mechanism of the surface carbon formation was determined, results for different metals were compared. Among Fe(111), Ni(100) and Ni(111) surfaces, Fe(111) surface was found to have lower activation barrier values. Performance of these catalysts can be asserted reversely proportional with the activation barrier values. Fe(111) lead lower activation barriers and its performance was better than other two surfaces. According to this information, Fe(111) surface was seen to be better catalyst than Ni(111) and Ni(100) surfaces for the surface nanocarbon formation. As it is stated in the literature survey part, dissociation of carbon source, which was studied in this work, is known to be the rate determining step for carbon nanotube formation mechanism. Hence result of the catalytic performance comparison in this study applies to the carbon nanotube formation. By using this fact, Fe(111) surface showed better performance than Ni(111) and Ni(100) surfaces for the carbon nanotube production. Also according to results of the experimental study conducted in Sabancı University by the supervision of Yuda Yürüm, it was found that Fe catalyst shows better activity that Ni catalyst for CCVD method with acetylene (Yürüm & Önal, 2010-2013). By these results, objectives of this study were achieved.

CHAPTER 6

RECOMMENDATIONS

In the future, this project can be used for further studies. For the recent researchers following items were recommended.

- Adsorption energies of additional acetylenes to the surface
- Simulations on Fe_3C surface
- Simulations on Co catalyst surface
- Simulations on bimetallic catalyst surfaces

Final structure obtained from the surface carbon synthesis studies can be taken and additional acetylene molecules can be adsorbed to the surface. With the dehydrogenation of these acetylene molecules, carbon nanotube growth may be investigated. Also adsorption energy profile for the further acetylene adsorptions may be generated. Actually part of this study was conducted with this study and obtained results were given in Appendix B.

In the literature survey part of the thesis metal carbides, Co catalyst and bimetallic catalysts were mentioned. These structures may be used for the future simulations for the nanocarbon synthesis works. Acetylene adsorption and dehydrogenation studies were also conducted during this work and obtained structure was given in Appendix B.

BIBLIOGRAPHY

Blöchl, P. E. (1994). Projector augmented-wave method. *Phys. Rev. B*, 17953.

Dasgupta, K., Joshi, J. B., & Banerjee, S. (2011). Fluidized bed synthesis of carbon nanotubes – A review. *Chemical Engineering Journal*, 841-869.

Endo, M., Strano, M. S., & Ajayan, P. M. (2008). Potential applications of carbon nanotubes. *Topics in Applied Physics*, 13-62.

Engel, E., & Dreizler, R. M. (2011). *Density functional theory: an advanced course.* Springer.

Filirri, C., Gonze, X., & Umrigar, C. J. (1996). Generalized gradient approximations to density functional theory: comparison with exact results. *Theoretical and Computational Chemistry*, 295-326.

Gasman, L. D. (2006). *Nanotechnology applications and markets.* Norwood: Artech House.

Heine, T., Joswig, J.-O., & Gelessus, A. (2009). *Computational chemistry workbook: learning through examples.* Weinheim: WILEY-VCH Verlag GmbH & Co. KGaA.

Hernadi, K., Fonseca, A., Nagy, J. B., Siska, A., & Kiricisi, I. (2000). Production of nanotubes by the catalytic decomposition of different carbon-containing compounds. *Applied Catalysis A: General*, 245-255.

Howard, P., Morris, G., & Sunley, G. (2007). Introduction: catalysis in the chemical industry. In G. P. Chiusoli, & P. M. Maitlis, *Metal-Catalysis in Industrial Organic Processes* (pp. 1-22). RSC Publishing.

Inglezakis, V. J., & Poulopoulos, S. G. (2006). *Adsorption, ion exchange and catalysis: design of operations and environmental applications.* Elsevier.

Institute for Theoretical Chemistry, University of Texas at Austin. (n.d.). *TRANSITION STATE TOOLS FOR VASP*. Retrieved December 2011, from NUDGED ELASTIC BAND: http://theory.cm.utexas.edu/vtsttools/neb/

Jensen, F. (2007). *Introduction to Computational Chemistry.* West Sussex: John Wiley & Sons Ltd.

Jeong, H. J., Kim, K. K., Jeong, S. Y., Park, M. H., Yang, C. W., & Lee, Y. H. (2004). High-yield catalytic synthesis of thin multiwalled carbon nanotubes. *The Journal of Physical Chemistry*, 17695-17698.

Joselevich, E. J., Dai, H., Liu, J., Hata, K., & Windle, A. H. (2008). Carbon nanotube synthesis and organization. *Topics in Applied Physics* , 101-165.

Journet, C., & Bernier, P. (1998). Production of carbon nanotubes. *Applied Physics A: Materials Science & Processing*, 1-9.

Kim, H., & Sigmund, W. (2005). Iron particles in carbon nanotubes. *Carbon*, 1743-1748.

Kresse, G., & Furthmuller, J. (1996). Efficiency of ab initio total energy calculations for metals and semiconductors using plane wave basis set. *Computational Materials Science*, 15-51.

Kresse, G., & Hafner, J. (1994). Ab initio molecular dynamics simulation of the liquid metal amorphous semiconductor transition in germanium. *Pyhs. Rev. B*, 14251.

Kresse, G., Marsman, M., & Furthmüller, J. (2011, 10). *VASP the GUIDE*. Retrieved 11 2011, from Vienna Ab-initio Simulation Package: http://cms.mpi.univie.ac.at/vasp/vasp/

Lewars, E. (2003). *Computational chemistry: introduction to the theory and applications of molecular and quantum mechanics.* Kluwer Academic Publishers.

Li, H., He, D., Li, T., Genestoux, M., & Bai, J. (2010). Chemical kinetics of catalytic chemical vapor deposition of an acetylene/xylene mixture for improved carbon nanotube production. *Carbon*, 4330-4342.

Loiseau, A., Blase, X., Charlier, J. -C., Gadelle, P., Journet, C., Laurent, C., et al. (2006). Synthesis methods and growth mechanisms. In A. Loiseau, P. Launois, P. Petit, S. Roche, & J. P. Salvetat, *Understanding carbon nanotubes from basics to applications* (pp. 49-130). Berlin: Springer-Verlag.

Lopez, P. N., Ramos, I. R., & Ruiz, A. G. (2001). A study of carbon nanotube formation by C_2H_2 decomposition on an iron based catalyst using a pulsed method. *Carbon*, 2509-2517.

Nagy, A. (1998). Density functional. Theory and application to atoms and molecules. *Physics Reports*, 1-79.

Neurock, M. (1997). Studies in surface science and catalysis. *dynamics of surfaces and reaction kinetics in heterogeneous catalysis* (pp. 3-34). Antwerp, Belgium: Elsevier.

Ni, L., Kuroda, K., Zhou, L. P., Kizuka, T., Ohta, K., Matsuishi, K. (2006). Kinetic study of carbon nanotube synthesis over Mo/Co/MgO catalysts. *Carbon*, 2265-2272.

Ni, L., Kuroda, K., Zhou, L. P., Ohta, K., Matsuishi, K., & Nakamura, J. (2009). Decomposition of metal carbides as an elementary step of carbon nanotube synthesis. *Carbon*, 3054-3062.

Page, A. J., Minami, S., Ohta, Y., Irle, S., & Morokuma, K. (2010). Comparison of single-walled carbon nanotube growth from Fe and Ni nanoparticles using quantum chemical molecular dynamics methods. *Carbon*, 3014-3026.

Parr, R. G., & Yang, W. (1994). *Density-functional theory of atoms and molecules.* Oxford University Press .

Patel, A., Prajapati, P., Chaudhari, K., Boghra, R., & Jadhav, A. (2011). Carbon nanotubes production, characterisation and its applications. *International Journal of Pharmaceutical Sciences Review and Research*, 74-80.

Perdew, J. P., Chevary, J. A., Vosko, S. H., Jacson, K. A., Peterson, M. R., Singh, D. J., (1992). Atoms, molecules, solids and surfaces: applications of the generalized gradient approximation for exchange and correlation. *Phys. Rev. B*, 6671.

Pirard, S. L., Douven, S., Bossuot, C., Heyen, G., & Pirard, J. P. (2007). A kinetic study of multi-walled carbon nanotube synthesis by catalytic chemical vapor deposition using a Fe–Co/Al2O3 catalyst. *Carbon*, 1167-1175.

Popov, V. N. (2004). Carbon nanotubes: properties and application. *Materials Science and Engineering*, 61-102.

Rode, B. M., Hofer, T. S., & Kugler, M. D. (2007). *The basics of theoretical and computational chemistry.* Weinheim: WILEY-VCH.

Rümmeli, M. H., Ayala, P., & Pichler, T. (2010). Carbon nanotubes and related structures:. In D. M. Guldi, & N. Martin, *Carbon nanotubes and related structures: synthesis, characterization, functionalization, and applications* (pp. 1-21). Wiley-VCH Verlag GmbH & Co. KGaA.

Seminario, J. M. (1995). An introduction to density functional theory in chemistry. In J. M. Seminario, & P. Politzer, *Modern Density Functional Theory: A Tool For Chemistry.* Elsevier Science.

Sholl, D. S., & Steckel, J. A. (2009). *Density functional theory: a practical introduction.* Wiley.

Smith, G. V., & Notheisz, F. (1999). *Heterogeneous catalysis in organic chemistry.* hardbound: ACADEMIC PRESS.

Terrones, H., & Terrones, M. (2007). The shape of carbon: novel materials for the 21st century. In A. G. Davies, *Advances in Nanoengineering : Electronics, Materials and Assembly* (pp. 7-32). Imperial College Press.

Tran, K. Y., Heinrichs, B., Colomer, J. F., Pirard, J. P., & Lambert, S. (2007). Carbon nanotubes synthesis by the ethylene chemical catalytic vapour deposition (CCVD) process on Fe, Co, and Fe–Co/Al2O3 sol–gel catalysts. *Applied Catalysis A: General*, 63-69.

Tsoufis, T., Xidas, P., Jankovic, L., Gournis, D., Saranti, A., Bakas, T. (2007). Catalytic production of carbon nanotubes over Fe–Ni bimetallic catalysts supported on MgO. *Diamond & Related Materials*, 155-160.

Turner, A. (2008). *Nanotechnology an Introduction.* Global Media.

Varga, K., & Driscol, J. (2011). *Computational Nanoscience: Applications for Molecules, Clusters, and Solids.* Cambridge.

Vesselenyi, I., Niesz, K., Siska, A., Konya, Z., Hernadi, K., Nagy, J. B., et al. (2001). Production of carbon nanotubes on different metal supported catalysts. *React.Kinet.Catal.Lett.*, 329-336.

Winter, M. (2010). *Iron: crystal structure*. Retrieved 10 2010, from WebElements: the periodic table on the web: http://www.webelements.com/iron/crystal_structure.html

Winter, M. (2010). *Nickel: crystal structure*. Retrieved 10 2010, from WebElements: the periodic table on the web: http://www.webelements.com/nickel/crystal_structure.html

Ying, L. S., Salleh, M. A., Yusoff, H. M., Rashid, S. B., & Razak, J. A. (2011). Continuous production of carbon nanotubes – A review. *Journal of Industrial and Engineering Chemistry*, 367-376.

Young, D. (2001). *Computational chemistry: a practical guide for applying techniques to real world problems.* Wiley.

Yu, Z., Chen, D., Totdal, B., Zhao, T., Dai, Y., Yuan, W. (2005). Catalytic engineering of carbon nanotube production. *Applied Catalysis A: General*, 223-233.

Yürüm, Y., Önal, I. (2010-2013). Investigation of the catalytic synthesis of carbon nanotubes with experimental methods and with quantum chemical theoretical techniques. Project 109M214, TUBITAK

APPENDIX A

SAMPLE VASP CODES

To be able to run VASP simulations four different input files should be used. These files are named as INCAR, KPOINTS, POSCAR and POTCAR files. Among these four files, INCAR file contains calculation parameters and simple comments. Simply it can be said that INCAR file determines what will be done for the computation. KPOINTS file includes information about the k-points as it can be understand from its name. POSCAR file supplies the geometry of the input structure that would be studied. It includes information about the lattice geometry, position of all atoms and data about which atoms are fixed and which ones are relaxed. POTCAR file for a simulation includes pseudopotential information about the atoms contained in the POSCAR file. Each atom has different POTCAR files generated for them. Thus POTCAR file should be generated by the addition of the POTCAR files of the atoms used in the simulation according to their order in the POSCAR file. Following sections of Appendix A gives example files for bulk relaxation, optimization, equilibrium geometry, CI-NEB and transition state calculations. For more detailed information official site of VASP may be visited (Kresse, et. al., 2011).

A1. Sample VASP Codes for Bulk Relaxation

A1.1. INCAR File

```
SYSTEM = Fe_BCC_Bulk
ISTART = 0
PREC   = HIGH
ISIF   = 3
IBRION = 2;
NFREE = 2;
NSW    = 150
LREAL  = .FALSE.
ISMEAR = 1;
SIGMA = 0.1;
LWAVE  = .False.
ENCUT  = 500
EDIFFG  = 1e-6
```

A1.2. KPOINTS File

```
K-Points
 0
Monkhorst Pack
19 19 19
0   0   0
```

A1.3. POSCAR File

```
Fe
2.8665
 -0.5  0.5  0.5
  0.5 -0.5  0.5
  0.5  0.5 -0.5
1
Selected Dynamics
Cartesian
     0    0    0    T T T
```

A2. Sample VASP Codes for Optimization (Equilibrium Structure) Calculations

A2.1. INCAR File

```
EDIFFG = -0.015
IBRION = 2;
!POTIM = 0.2;
!NFREE  = 20
ISMEAR = 1;
SIGMA = 0.2;
LREAL = Auto
ENCUT  = 500
IDIPOL = 3
LDIPOL = .TRUE.
NSW    = 300
ALGO=FAST
```

A2.2. KPOINTS File

```
K-Points
 0
Monkhorst Pack
 4  4  1
 0  0  0
```

A2.3. POSCAR File

Fe C H
1.00000000000000
6.7523134709999999 -3.8984500000000000 0.0000000000000000
0.0000000000000000 7.7968999999999999 0.0000000000000000
0.0000000000000000 0.0000000000000000 13.9787999999999997
24 2 2
Selective dynamics
Cartesian

1.1254080900	1.9491860200	0.0000000000	F F F
1.1254080900	5.8476360200	0.0000000000	F F F
4.5015648200	-0.0000389800	0.0000000000	F F F
4.5015648200	3.8984110200	0.0000000000	F F F
2.2459894400	-0.0156691600	1.0313625100	T T T
2.2508547700	3.8910432900	1.0244585400	T T T
5.6264864600	-1.9577812200	1.0241968000	T T T
5.6269204400	1.9414324300	1.0245112300	T T T
-0.0045753500	-0.0054265500	1.0323149600	T T T
-0.0007830800	3.8888960500	1.0296691100	T T T
3.3800005200	-1.9591376400	1.0320273000	T T T
3.3703089500	1.9321776600	1.0357920300	T T T
1.1408709900	1.9574304000	2.2107276500	T T T
1.1225183000	5.8301366000	2.2183691200	T T T
4.5119733000	0.0113184400	2.2105095700	T T T
4.4858028500	3.8579166400	2.1836631300	T T T
2.2169550200	-0.0734345800	3.3258554100	T T T
2.2076638500	3.9049508400	3.3743538500	T T T
5.6279808800	-1.9568612400	3.3114624900	T T T
5.6653196000	1.9083789000	3.3727173600	T T T
-0.0127623700	0.0074492200	3.3261323100	T T T
-0.0018686200	3.8821458700	3.3343825400	T T T
3.4012147100	-1.9648640900	3.3264732500	T T T
3.2687625000	1.7505797600	3.4216704400	T T T
2.9968548100	3.0462252900	4.4319357700	T T T
4.2084576700	2.3464373800	4.4276161100	T T T
2.4626308600	3.2008084900	5.3846338900	T T T
4.6143841500	1.9586828800	5.3771541700	T T T

A3. Sample VASP Codes for CI-NEB Calculations

A3.1. INCAR File

```
!FOR Fe NEB
IMAGES = 8
SPRING = -5
ICHAIN = 0
LCLIMB = .TRUE.
LTANGENTOLD = .FALSE.
LDNEB  = .FALSE.
!EDIFFG = -0.015
IBRION = 1;
POTIM = 0.2;
!NFREE  = 20
NSW    = 100
LDIPOL = .TRUE.
ISMEAR = 0; SIGMA = 0.1;
LREAL = Auto
ENCUT  = 500
IDIPOL = 3
LCHARG = .FALSE.
ALGO=FAST
```

A3.2. KPOINT File

```
K-Points
 0
Monkhorst Pack
 4  4  1
 0  0  0
```

A4. Sample VASP Codes for Transition State Calculations

A4.1. INCAR File

```
SYSTEM = Ni C H
!ISTART = 0
!PREC   = HIGH
!ISIF   = 2
IBRION = 1; NFREE = 20;
NSW    = 150
LREAL  = AUTO
ISMEAR = 1; SIGMA = 0.2;
ENCUT = 500
IALGO = 48
!EDIFFG = -0.01
!IDIPOLE = 3
!LDIPOLE = .TRUE.
```

A4.2. KPOINTS File

```
K-Points
 0
Monkhorst Pack
 4  4  1
 0  0  0
```

A5. Sample VASP Codes for Vibrational Frequency Calculations

A5.1. INCAR File

```
PREC   = HIGH
ISYM=0
EDIFFG = -0.015
EDIFF = 1e-6
IBRION = 5;
POTIM = 0.02;
!NFREE  = 20
ISMEAR = 0;
SIGMA = 0.1;
LREAL = Auto
ENCUT  = 500
NSW    = 900
LDIPOL = .TRUE.
IDIPOL = 3
LCHARGE = .FALSE.
ALGO=FAST
```

A5.2. KPOINTS File

```
K-Points
 0
Monkhorst Pack
 4  4  1
 0  0  0
```

APPENDIX B

FURTHER ACETYLENE ADSORPTION ON Fe(111) SURFACE

Acetylene adsorption and dehydrogenation was studied for Fe(111), Ni(111) and Ni(100) surfaces. However it was useful to check the behavior of the surface for the further acetylene adsorption(s). For this purpose Fe(111) was selected, two additional acetylene molecules were adsorbed to surface one by one. In order to conduct this study direct hydrogen-hydrogen interaction method was used to dehydrogenate acetylene molecules. Reason of selecting direct hydrogen-hydrogen interaction method will be explained at the end of this section. Final structure from the mechanisms studied for this thesis project was taken and hydrogens were completely removed. Then second acetylene was adsorbed on this structure. After the adsorption process, hydrogens of the second acetylene were removed to gas phase by direct hydrogen-hydrogen interaction method. After hydrogens of the second acetylene were removed, the third acetylene was adsorbed to the surface. Obtained adsorption values were used to generate Figure B1. According to Figure B1, it may be said that the amount of surface carbon reduced the amount of adsorption energy of acetylene. This may be caused from the decrease in the available free metal sites on the surface. Structure obtained after this additional study is given in Figure B2.

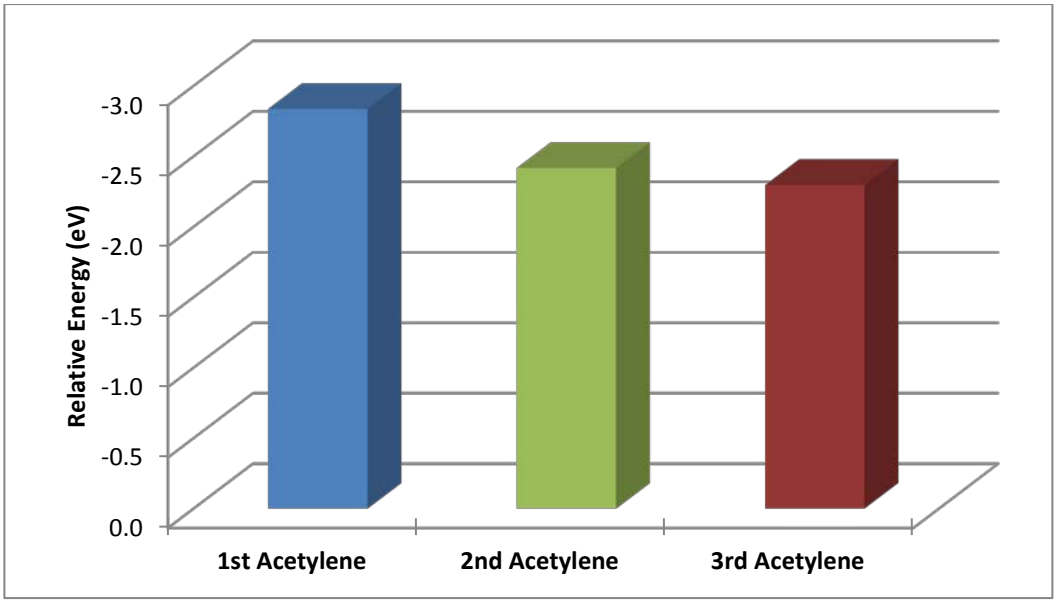

Figure B1: Adsorption energies of acetylenes to the surface.

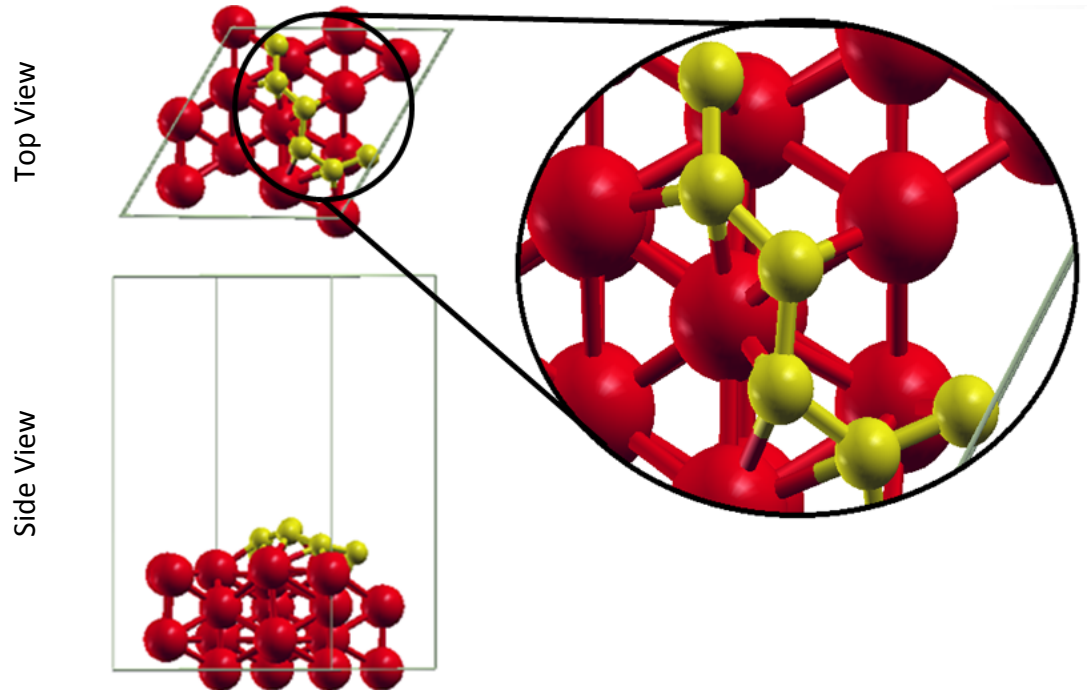

Figure B2: Structure obtained after 3 adsorption and dehydrogenation of three acetylene

After obtaining the structure in Figure B2, one more acetylene molecule was adsorbed to the surface and the new structure was shown in Figure B3. If this new structure was examine it can be seen that the structure has the configuration of one side of armchair carbon nanotube.

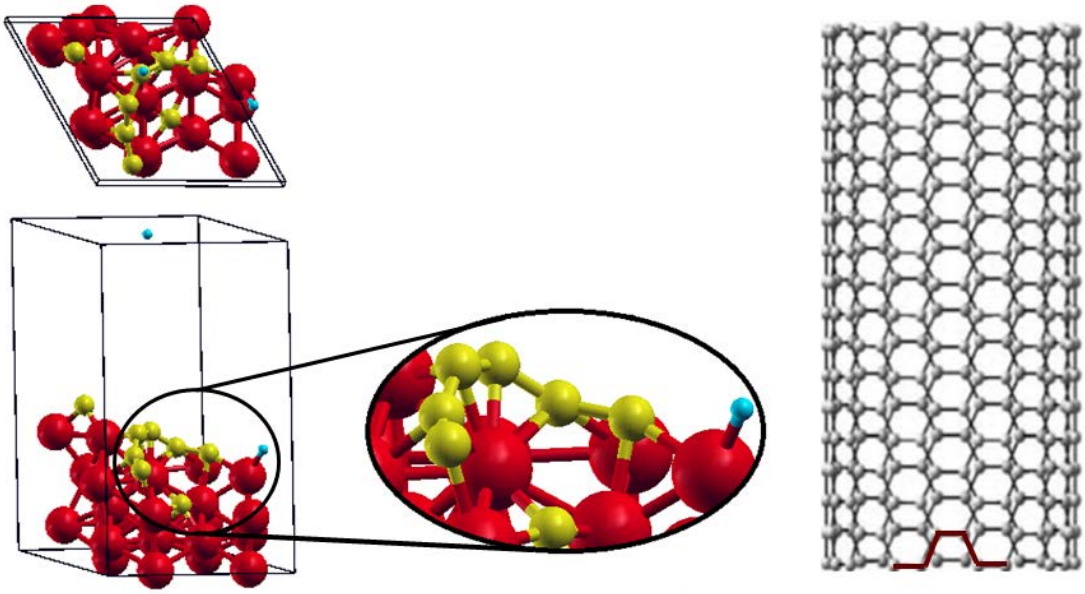

Figure B3: Structure obtained after adsorption of the 4th acetylene

Finally acetylene adsorption studies on the Fe_3C slab were conducted and structure shown is the Figure B4 was obtained. This structure may be used for carbon nanotube growth studies.

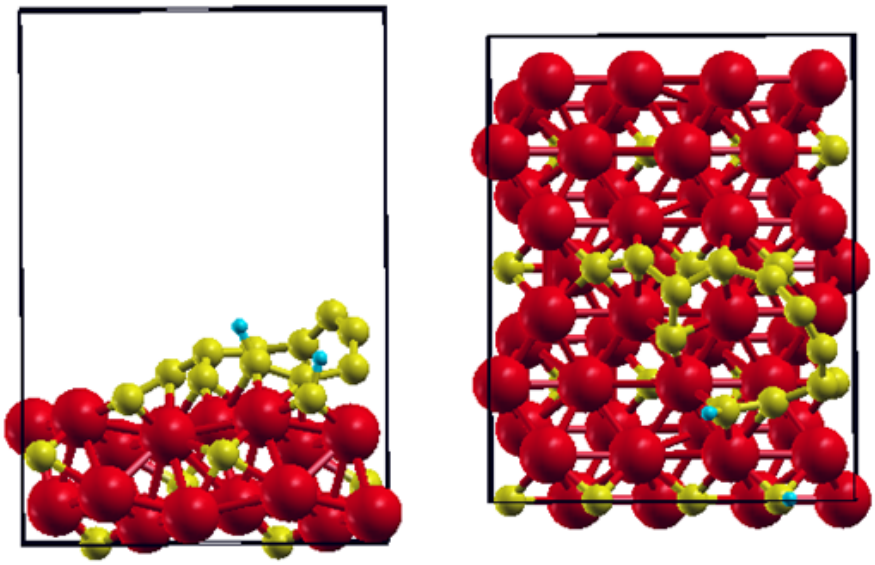

Figure B4: Structure obtained after acetylene adsorption and dehydrogenation studies on Fe_3C slab.

Reasons of choosing hydrogen-hydrogen interaction method for additional studies can be stated as:

- All of studied there methods gave same output according to structure geometry and energy value.
- Only differences between methods studied were number of steps of the mechanism and activation barriers on the pathway.
- Acetylene adsorption was independent of mechanisms studied.

According to above three item, hydrogen-hydrogen interaction method was the best choice. Hence, hydrogen-hydrogen interaction method requires less computational effort than the other two methods and only acetylene adsorption was the only subject of interest for this part of the study and dehydrogenation details were not required.